

Femtosecond Time-Resolved Single-Shot Optical Kerr Effect Measurements

A dissertation

submitted to Tokushima University

for the degree of Doctor of Philosophy in

Optical Systems Engineering

September 2016

Xiaofang Wang

Femtosecond Time-Resolved Single-Shot Optical Kerr Effect Measurements

by

Xiaofang Wang

Submitted to Department of Optical Systems Engineering in July 2016
in fulfillment of the requirements for the degree of
Doctor of Philosophy

Abstract

Femtosecond time-resolved pump-probe optical Kerr gating (OKG) measurements, have many advantages, such as high time resolution (~ 100 fs), high signal-to-noise ratio, and without the need for phase matching. Therefore, they have been widely used in various areas, such as measurements of third-order nonlinear optical properties, ultrafast fluorescence spectroscopy, ballistic imaging, etc. Femtosecond time-resolved optical polarigraphy technique (FTOP), based on OKG, can be used to directly observe the instantaneous intensity distributions of ultra-short pulses propagating in transparent mediums with two-dimensional spatial distribution. However, the traditional pump-probe technique is not suitable for monitoring irreversible process owing to sample depletion, product accumulation or pulse fluctuation. Therefore, it is necessary to develop single-shot pump-probe techniques, which can also be used for single-shot imaging of ultrashort pulses propagation.

In this thesis, two ultrafast time-resolved single-shot imaging techniques of femtosecond pulse propagating in transparent media have been investigated, one

based on supercontinuum probing, and the other by introducing an echelon into the probe path. The influence of response time of optical Kerr media on imaging has been investigated. Based on nonlinear ellipse rotation, we proposed an OKG measurement using an elliptically polarized probe beam, in which OKG signal is independent on the pump polarization. In addition, the pump power dependence of the spatial gating properties of femtosecond OKG was investigated. The main creative and innovative research results are listed as follows

1. We investigated the ultrafast time-resolved single-shot imaging of femtosecond pulse propagation using a supercontinuum and FTOP in transparent liquids. The supercontinuum probe senses the instantaneous birefringence induced by the laser pulse, and a FTOP image with different color distributions could be obtained. By comparing the wavelength distributions and the saturation variation of the images, the recorded FTOP images in two samples with different response time were analyzed. In the fast response sample, N-methyl-2-pyrrolidone (NMP), the spectral widths and the saturation values of the FTOP image at fixed positions were narrower and higher than those in CS₂. Due to the slow response of CS₂, the probe light sensed a long-lived birefringence and the FTOP image contained more wavelength components at every position along the pump pulse propagation direction.

2. We have demonstrated high-frame-rate observations of a single femtosecond laser pulse propagating intransparent medium using the FTOP technique and an echelon. The echelon produced a spatially encoded time delay for the probe pulse to capture directly four successive images of an intense propagating pulse with picosecond time

interval and femtosecond time resolution. Using this method, we observed the propagation process of a single femtosecond laser pulse in fused silica with 280 fs time resolution and 1.05 THz frame rate. The influence of pulse-energy fluctuation on the spatial and temporal distribution of the single laser pulse was visualized using the single-shot measurements.

3. The pump power dependence of the spatial gating properties of femtosecond OKG was investigated using coaxial two-color optical Kerr measurements in CS_2 . As the pump power increased, the spatial pattern of the optical Kerr signals changed from a Gaussian spot to a ring form, and then a spot surrounded by a concentric ring, successively. By comparing the experimental data with the calculation results and measuring the pump power dependence of the OKG signal intensity, we demonstrated that the spatial variation of OKG transmittance could be attributed to the non-uniform spatially distributed phase change of the probe beam, due to the transient birefringence effect induced by pump beam with transverse mode of a Gaussian distribution.

4. Based on light-induced polarization ellipse rotation effect, we proposed an ultrafast OKG in which an elliptically polarized probe beam was used by introducing a pair of crossed quarter-wave plates before and after the Kerr medium in a conventional OKG arrangement. When the probe beam passed through the Kerr medium, a rotation of the polarization ellipse of the probe beam would occur due to the transient birefringence induced by the pump beam, and parts of the probe beam would pass through the OKG. Theoretical calculations and experimental results indicated that the OKG signal

intensity would reach an optimum value and be pump-polarization independent when the probe beam were circularly polarized.

KEY WORDS: Femtosecond laser, Optical Kerr gate, Single-shot measurements

TYPE OF DISSERTATION: Application Fundamentals

Acknowledgements

During my enjoyable graduate life, I owe a great deal of thanks to many people who have made it possible for me to do the work presented here.

I would like to deeply thank my advisors Prof. Si at Xi'an Jiaotong University, China, and Prof. Matsuo at Tokushima University, Japan, for all their have done for me. If without their rich knowledge, close guidance and endless support, I would never have finished.

I would also like to thank Prof. Hashimoto, who offered me a lot of help whenever I needed in Japan, and made me feel like a family member.

Many thanks shall be paid to Prof. Yan for teaching me many tricks on experimental operation, and how to write academic paper. He always made me feel working in the lab is a wonderful thing.

I am also appreciative of the help from Asada-san, Zhang-san, Kang-san in CICEE and all the members in International Center of Tokushima University, and financial support of JASSO scholarship.

There are many interesting and multi-talented lab members who have become my friends. Their kindness and unconditional support have contributed a great part to my graduate student life.

Acknowledgements

Finally, I want to express my deepest appreciation to my parents, my sister, and my husband. Their support, love and encouragement made all of this possible.

Contents

Chapter 1 Introduction	14
1.1 Motivation.....	14
1.2 Objectives	16
1.3 Thesis Outline	17
Chapter 2 An Introduction to Single-Shot Pump-Probe Spectroscopy and OKG Measurements	19
2.1 Single-Shot Pump-Probe Spectroscopy	19
2.1.1 Pump-Probe Spectroscopy	19
2.1.2 Supercontinuum Probing	22
2.1.3 Using Echelon Mirrors.....	25
2.2 OKG Measurements.....	26
2.2.1 The principle of OKG measurements	26
2.2.2 FTOP Technique	29
2.3 Summary	32
Chapter 3 Ultrafast Single-Shot Imaging of Femtosecond Pulse Propagation in Transparent Liquids Using FTOP and a Supercontinuum	34
3.1 Introduction.....	34
3.2 Experimental methods	36
3.3 Results and discussion	38
3.4 Summary	42
Chapter 4 High-Frame-Rate Observation of Single Femtosecond Laser Pulse Propagation in Fused Silica Using FTOP and an Echelon.....	44
4.1 Introduction.....	44
4.2 Experimental methods	45
4.3 Results and Discussions	48
4.4 Summary	52
Chapter 5 Pump Power Dependence of the Spatial Gating Properties of Femtosecond OKG Measurements.....	53
5.1 Introduction.....	53
5.2 Experimental methods	54
5.3 Results and discussion	56
5.4 Summary	61
Chapter 6 An Ultrafast OKG Measurement Based on Light-induced Polarization Ellipse Rotation.....	62
6.1 Introduction.....	62
6.2 Experimental methods	63
6.3 Theoretical calculations	64

6.4	Experimental results and discussion	67
6.5	Summary	69
Chapter 7	Conclusions	70
7.1	Contributions.....	70
7.2	Future Work	72
Bibliography	73

List of figures

Figure 2-1: Schematic of pump-probe spectroscopy. The output femtosecond laser pulse is split into a intense pump and a weak probe beams. The intense pump beam is used to excite the sample, and the probe beam is used to probe, which is collected by a detector after passing through the sample. The delay line is used to adjust the optical path difference between the pump and probe.20

Figure 2-2: (a) Experimental setup of single-shot pump-probe spectorscopy using a cylindrical lens to focus the pump and probe beams into the sample with different delay time and frequency at different focus place, here the probe is normal incidence and the pump is oblique incidence; (b) an experimental single-shot trace [59]21

Figure 2-3: A supercontium spectrum generated in air by 800-nm, 70-fs laser pulses[82].....23

Figure 2-4: Three-dimensional shape measurement of objects using a supercontium [110].....24

Figure 2-5: A draft of an echelon which is an optic with plenty of stair steps, which can subdivide the transverse profile of a probe beam into multiple distinct pulses, each with a different delay time and reach the sample at a different time.25

Figure 2-6: Schematic of dual-echelon single-shot femtosecond spectroscopy [113].26

Figure 2-7: A schematic of OKG setup. The OKG is made up of a Kerr medium and two crossed polarizers placed before and after the Kerr medium. Without the pump beam, the probe beam can not pass through the analyzer. OKG is off. And when the pump and probe beams pass through the medium at the same time and overlapped with each other, the pump beam will induce a birefringence of the Kerr medium , and

the polarization of the probe beam will change from a linealy polarized light to an elliptically polarized light. Thus part of the probe beam can pass through the crossed analyzer and can be detected. At this time, the OKG is open.27

Figure 2-8: Kerr efficiency of quartz and SFL-6 dependence of the gate intensity [122]29

Figure 2-9: The schematic of FTOP. The single-headed arrows indicate the propagation directions of the pump and probe pulses. The double-headed arrows indicate the polarization direction of the pulses which are both linearly polarized. According to the optical Kerr effect, when the intense femtosecond laser pulse popagating in the medium, it would induce anisotropic change of refractive index in the medium in proportion to its intensity distribution [47].31

Figure 3-1: Time-resolved measurements of OKG signals for NMP and CS₂. The red circles and the black squares are the experimental data of NMP and CS₂, respectively. The red solid curve indicates the Gaussian fit of NMP. The black curve of CS₂ is fitted by a bi-exponential decay function with time constants 160 fs and 1.6 ps.36

Figure 3-2: Experimental setup for FTOP, where a supercontinuum generated in water was used as the probe light. BS: beam splitter, M: mirror, ND: neutral density filter, A: aperture, L: lens, FS: fused silica, F: short-wave pass filter, P: polarizer, and HWP: half-wave plate.38

Figure 3-3: Imaged filaments induced by a femtosecond laser pulse in (a) NMP and (b) CS₂, the CCD exposure times are 1/6 s and 1/75 s, respectively. Distance means the propagation distance of the pump pulse in the irradiated range of the supercontinuum. Chirp character of the supercontinuum (red circles) and wavelength distributions of the recorded images (black squares) in (c) NMP and (d) CS₂.39

Figure 3-4: The spectra of the FTOP images along the pulse propagation direction detected by fiber optic spectrometer behind the analyzer (P2).....41

Figure 3-5: The saturation of the FTOP images along the pulse propagation direction. The inset shows the corresponding hue of the images.....42

Figure 4-1: Experimental setup of multi-frame FTOP imaging technique using an echelon. BS: beam splitter, ND: neutral density filter, M: mirror, L: lens, FS: fused silica; P: polarizer, HWP: half-wave plate.....46

Figure 4-2: Schematic of FTOP using an echelon, in the upper right corner is a side view of setps of an echelon.....47

Figure 4-3: Four-frame observation of pulse propagation in fused silica using 100 pulses of 15 μ J. The pulse propagated from left to right.48

Figure 4-4: Exposure intensity distribution of the four-frame FTOP image as a function of the propagation time of the pump pulse. The solid lines show the Gaussian fit curves.....50

Figure 4-5: Single-shot four-frame observation of single 45 μ J pulse propagation in fused silica. The pulse propagated from left to right. (a)-(d) correspond to different laser shots under the same conditions.....51

Figure 4-6: Intensity distributions of the first frames of the single-shot images shown in Figure 4-4(a)-(d). (A) Along the pulse propagation direction, and (B) along the transverse direction.52

Figure 5-1: Scheme of the experimental setup. BS: beam splitter; DM: dichroic mirror; HWP: half-wave plate; P: polarizer; F: bandpass filter.55

Figure 5-2: OKG signal profile when the pump fluence was fixed at (a) 1.63 mJ/cm^2 , (b) 3.39 mJ/cm^2 , (c) 4.53 mJ/cm^2 , (d) 8.53 mJ/cm^2 , and (e) 10.46 mJ/cm^2 , respectively.

.....56

Figure 5-3: One-dimensional OKG signal intensity distributions when the pump fluence was fixed at (a) 1.63 mJ/cm², (b) 3.39 mJ/cm², (c) 4.53 mJ/cm², (d) 8.53 mJ/cm², and (e) 10.46 mJ/cm², respectively. The discrete solid points are experimental results. The red solid lines indicate the calculated curves.58

Figure 5-4: Pump fluence dependence of (a) spatially integrated exposure intensity of OKG signals and (b) OKG signals at $r=0$,. The squares are experimental results. The red solid line indicates the calculated curves.59

Figure 5-5: Polarization dependence of OKG signals, when the pump fluence was adjusted to 3.22 mJ/cm² and 10.30 mJ/cm², respectively. The squares and triangles are experimental results. The red solid line indicates the theoretical curve. The experimental results and the theoretical curve were both normal.....61

Figure 6-1: (a) Experimental arrangement for an OKG using an elliptically polarized probe beam. P: polarizer; H: $\lambda/2$ plate; Q: $\lambda/4$ plate; L: lens; PMT: photomultiplier tube. (b) The geometry of the fields and the axes of the wave plates. x and y axes are fast and slow axes of Q1, respectively. Eprobe is the probe field after H1 at angle α with respect to the fast axis of Q1. Epump is the pump field after H2 at angle β with respect to the fast axis of Q1.....64

Figure 6-2: Theoretical calculation result of the OKG signal intensity based on light-induced polarization ellipse rotation using Eq. (6-5)66

Figure 6-3: Time-resolved measurements of OKG signals in CS₂. The red open circles refer to the OKG signals using elliptically polarized probe light; the black solid squares as a reference refer to the general OKG signals using linearly polarized probe light.67

Figure 6-4: (a) Pump polarization direction dependence of OKG signal intensity under different polarization states of the probe beam. (b) Probe beam polarization state dependence of OKG signal intensity under different pump polarization directions. Scatter plots are experimental results; solid lines are fitted curves using Eq. (6-5). ...69

Chapter 1

Introduction

1.1 Motivation

About ultrafast time-resolved measurements, for different time resolution, there are different methods. Multiple physical processes, especially micro-phenomenon, occur at picosecond to femtosecond scale, such as chemical bond breaking and combining, intramolecular energy transfer, carrier dynamics, etc. To study such ultrafast processes, picosecond to femtosecond time resolution is needed. Electronic detectors, however, the resolution of which is about millisecond to nanosecond, can not achieve this goal. The advent of ultrafast laser makes it possible to use light sources instead of electronic detectors to measure the ultrafast processes. And compared with the electronic detector, the optical measurements with ultrafast laser pulse are more effective, with lower noise, and the time resolution is determined by the laser pulse duration. During the femtosecond range, the most useful method is pump-probe spectroscopy.

The OKG measurement, one of pump-probe spectroscopy, has been developed about half a century since it was first proposed in 1969 [1]. For the last few decades,

femtosecond OKG technique has been developed as one of the most effective methods for ultrafast phenomenon detection. This technique could provide an ultrafast measurement of high time resolution (~ 100 fs), high signal-to-noise ratio, and without the need for phase matching. Hence, it has been widely used in various ultrafast measurements, such as measurement of the third-order nonlinear response of all kinds of materials [2-4], ultrafast fluorescence spectroscopy [6-8], ballistic optical imaging [9-12], simultaneous three-dimensional (3-D) imaging [13-15], etc.

Femtosecond laser pulse [16-18] as the light source has two features: ultrashort laser pulse duration and ultrahigh peak power. First its pulse duration is about femtosecond, so it can realise femtosecond time resolution; second its peak power can reach terawatt, so it is suitable for exciting sample. With these two features, femtosecond laser pulses are widely used in transient spectroscopy [19-21], micro-imaging [22,23], terahertz imaging and spectroscopy [24-27], micromachining [28,29], etc. The advent of femtosecond laser necessitates the research of the propagation characteristics of ultrashort and intense laser pulses, which involves various self-modulating nonlinear effects [30,31]. And the propagation mode of laser filamentation has aroused a great interest due to its numerous potential applications, such as white light continuum light detection and ranging techniques [32-34], atmospheric application [35-37], lightning protection [38-40], generation of terahertz radiation [41], etc. In the past few years, various methods have been developed to research the propagation behaviors of intense laser pulses in transparent media, like holography, shadow-imaging, three-dimensional imaging etc [42-46]. FTOP, one of OKG measurements, is a direct method for observing the pulse propagation of a focused femtosecond laser [47-49]. However, the traditional FTOP method can hardly

obtain the whole map of a single pulse's propagation instantaneously, as amount of snapshot images are needed to be stacked to display the whole image. Because these images are taken using a serial of independent pulses, it cannot fulfill the single-shot measurements of the spatial propagation distribution of an intense light pulse, while single-shot technique is especially important for the research of irreversible effect of the intense pulse with the propagation medium. Therefore, it is necessary to develop single-shot pump-probe techniques, which can also be used for single-shot imaging of ultrashort pulses propagation.

1.2 Objectives

The purpose of this thesis is to investigate the single-shot imaging of a femtosecond laser pulse propagation in transparent media by OKG measurements, and develop the OKG measurements. The research topics in this thesis are:

- **Development of an ultrafast time-resolved single-shot imaging of femtosecond pulse propagation in transparent liquids using a supercontinuum and FTOP:** Combining the technique of FTOP with a supercontinuum, a single-shot imaging of a femtosecond pulse propagation in transparent media is realized. The influence of response time in different propagation media is studied.
- **Demonstration of high-frame-rate observations of a single femtosecond laser pulse propagating in transparent medium using an echelon and FTOP:** The echelon is produced with a spatially encoded time delay for the probe pulse to capture directly four successive images of an intense propagating pulse with picosecond time interval and femtosecond time

resolution. Using this method, the propagation process of a single femtosecond laser pulse in fused silica is observed. The influence of pulse-energy fluctuation on the spatial and temporal distribution of the single laser pulse is analyzed.

- **Investigation of the pump power dependence of the spatial gating properties of femtosecond OKG:** The spatial pattern of the OKG signals changed as the pump power increased is observed. Theoretical calculation results is obtained, and compared with the experimental data. The reason of spatial variation of OKG transmittance with the increase of the pump power is demonstrated.
- **Development of an ultrafast OKG based on light-induced polarization ellipse rotation effect:** Introducing a pair of crossed quarter-wave plates before and after the Kerr medium in a conventional OKG arrangement, an OKG using elliptically polarized probe beam is proposed and realized. The OKG signal intensity would reach an optimum value and be pump-polarization independent when the probe beam were circularly polarized is demonstrated by both theoretical calculations and experimental results.

1.3 Thesis Outline

Following the motivation and objectives presented in Chapter 1 , Chapter 2 reviews the literature on single-shot pump-probe spectroscopy, and introduces the principle of OKG. Chapter 3 presents the ultrafast time-resolved single-shot imaging of femtosecond pulse propagation in transparent liquids using a supercontinuum and

FTOP. Chapter 4 demonstrates the high-frame-rate observations of a single femtosecond laser pulse propagating in transparent medium using an echelon and FTOP. In chapter 5 the pump power dependence of the spatial gating properties of femtosecond OKG is investigated. In chapter 6, the ultrafast OKG based on light-induced polarization ellipse rotation effect is illuminated. In Chapter 7, a summary of the research contributions of this thesis and suggestions for future research is provided.

Chapter 2

An Introduction to Single-Shot Pump-Probe Spectroscopy and OKG Measurements

2.1 Single-Shot Pump-Probe Spectroscopy

2.1.1 Pump-Probe Spectroscopy

In the pump-probe spectroscopy (Figure 2-1), the output femtosecond laser pulse is split into an intense pump and a weak probe beams. The intense pump beam is used to excite the sample, and the probe beam is used to probe, which is collected by a detector after passing through the sample. The delay line is used to adjust the optical path difference between the pump and probe beams, that is, to adjust the delay time between the pump and probe beams. The pump beam would induce some changes in the sample. Hence, the probe beam passing through the sample would sense the changes, and then its intensity may be enhanced or attenuated, or its polarization state may be changed, or be diffracted, etc. By adjusting the delay line to record the information of probe beam at different fixed delay time, the dynamics processes of the

exciting sample can be obtained.

There are various kinds of pump-probe spectroscopy based on different transient physical effects, including absorption [50-52], fluorescence [53,54], four-wave-mixing [55,56], polarization rotation [57,58], etc. Here, the pump-probe spectroscopy we focus on is OKG based on optical Kerr effect (polarization rotation), which will be introduced in detail in section 2.2.

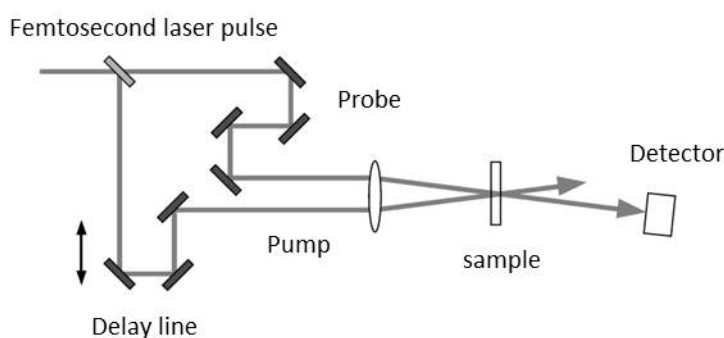


Figure 2-1: Schematic of pump-probe spectroscopy. The output femtosecond laser pulse is split into a intense pump and a weak probe beams. The intense pump beam is used to excite the sample, and the probe beam is used to probe, which is collected by a detector after passing through the sample. The delay line is used to adjust the optical path difference between the pump and probe.

In the traditional pump-probe spectroscopy, the transient information of the probe beam at a fixed delay time is obtained by adjusting the delay line at a fixed place. Here the output femtosecond laser pulses have to be supposed to be identical and induce identical physical processes in the sample, cause the transient information of different delay time is actually induced by different femtosecond laser pulse. However, to some of irreversible light-induced processes (such as organic crystalline reaction dynamics, light-induced breakdown), sample depletion, product accumulation and pulse fluctuation have greatly restricted the range of environments

amenable to study. To overcome this difficulty, single-shot pump-probe spectroscopy, monitoring the reaction in a single laser shot, is imperative.

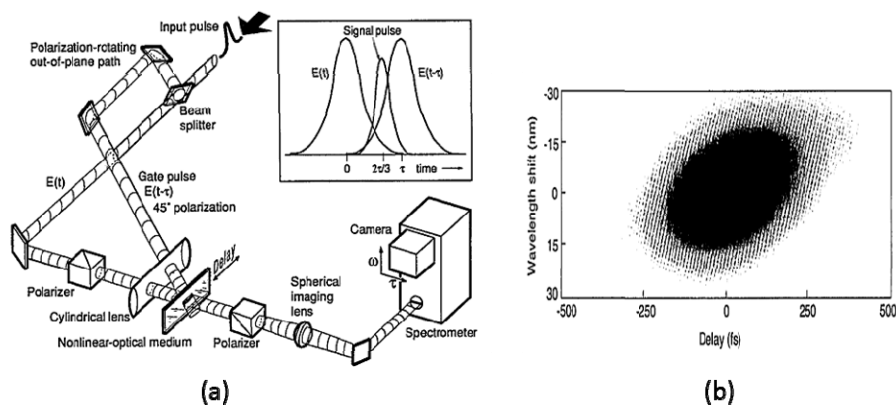


Figure 2-2: (a) Experimental setup of single-shot pump-probe spectroscopy using a cylindrical lens to focus the pump and probe beams into the sample with different delay time and frequency at different focus place, here the probe is normal incidence and the pump is oblique incidence; (b) an experimental single-shot trace [59]

Femtosecond time-resolved single-shot pump-probe spectroscopy can realize real-time measurements of ultrafast photochemical reaction, avoiding the influence of environment variation, sample depletion, product accumulation and pulse fluctuation on the traditional pump-probe measurements. A simple single-shot pump-probe measurement is using a cylindrical lens to focus the pump and probe beams into the sample (nonlinear-optical medium) with different delay time and frequency at different focus place, see Figure 2-2(a), here the probe is normal incidence and the pump is oblique incidence [59]. In the sample, in a direction parallel to the axis of the cylindrical lens, the probe is with the same delay time for normal incidence, while the pump beam is with different delay time for oblique incidence. Thus, it can realize time-resolved single-shot imaging. In the sample, in a direction both perpendicular to

the axis direction of the cylindrical lens and probe beam propagation direction, the different wavelength components of the laser pulse with different refractive index will be focused at different place. Thus it can realize frequency-resolved imaging. Figure 2-2(b) shows an experimental single-shot trace with time and frequency resolution. Using this single-shot measurement, a fair amount of work has done, such as studying the femtosecond pulse properties [60-65], terahertz pulse propagating in the air [66], fluorescence measurements [67], spectral measurement [68,69], etc. However, this is a measurement with small dynamic range, and high homogeneity of laser pulse and sample, high contact ratio of the pump and probe beams are required. Therefore, this single-shot pump-probe measurement can not apply to the ultrafast dynamics with large dynamic range or complex reaction. Besides, there are some other femtosecond time-resolved single-shot measurements based on X-ray diffraction [70-72], tomography [73-75], electro-optic sampling [76-78], or other techniques.

2.1.2 Supercontinuum Probing

White-light supercontinuum, or supercontinuum, with spectral width from infrared to ultraviolet, is generated when ultrashort laser pulses propagating in transparent medium. It is a combined result of multiple nonlinear optical effects induced by the ultrashort laser pulses including self-phase modulation, self-focusing, self-steepening, multi-photon absorption, plasma scattering, stimulated raman scattering, etc.

Supercontinuum was first observed in 532-nm picosecond laser pulses propagating in crystals and glasses in 1970, the linewidth was broadened to 400~700 nm with white light [79,80]. In 1999, S L Chin et al. demonstrated that a supercontinuum is indeed an ultrafast white light laser by femtosecond laser pulses in water, CH₄ and CCl₄ [81]. Figure 2-3 is a supercontinuum spectrum generated in air by

800-nm, 70-fs laser pulses [82].

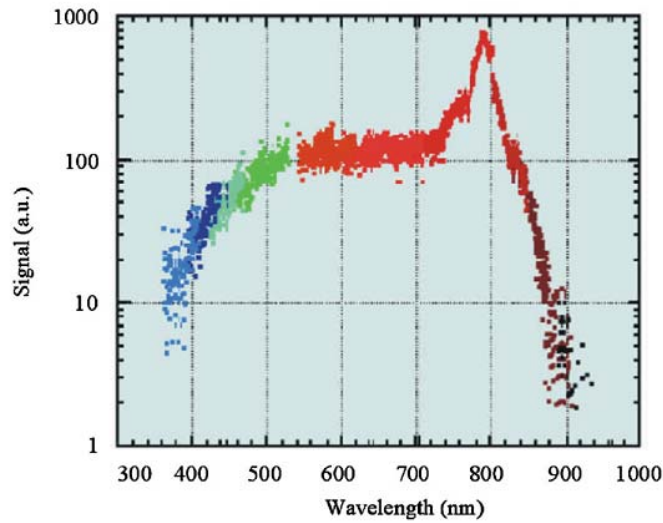


Figure 2-3: A supercontinuum spectrum generated in air by 800-nm, 70-fs laser pulses[82]

White-light supercontinuum can be generated in various kinds of materials, such as gas, liquid, block glasses, crystals, optical fibers and so on [83-89]. Supercontinuum generation by femtosecond laser pulses has some advantages, like high brightness, high directionality, and different spectral components with definite phase relationship; hence, it is indeed an ultrafast laser source. Compared with other ultrafast laser, white light supercontinuum is of wide bandwidth, high coherent, and easy to extract multiple wavelength components. Therefore, it has been used in atmospheric remote sensing [90-92], optical coherence tomography [93,94], ultra-short pulse compression [95,96], three-dimensional imaging [97], broadband optical fiber communication [98], and other significant areas.

Single-shot pump-probe spectroscopy based on supercontinuum, is a time- and frequency-resolved technique using a supercontinuum with chirp characteristic induced by ultrashort laser pulses in transparent medium as the probe beam. Because of chirp characteristic, the supercontinuum components of different wavelength is of different

delay time, thus they could sense the transient information in the sample at different delay time in a single shot. Therefore, it does apply to the measurements of ultrafast dynamic processes [99-104], like solvent effects on the excited-state processes of protochlorophyllide [105,106], ultrafast electron transfer dynamics [107,108], exciton dynamics and so on [109].

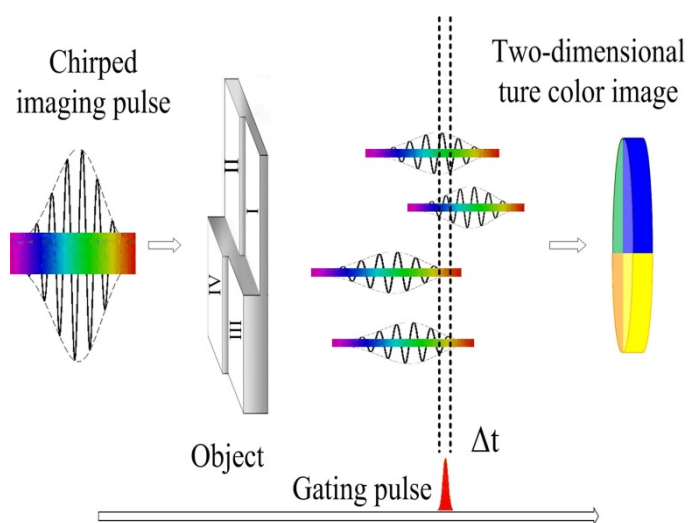


Figure 2-4: Three-dimensional shape measurement of objects using a supercontinuum [110]

Figure 2-4 shows a schematic of three-dimensional shape measurement of objects using a supercontinuum and OKG [93,110]. Because of chirp characteristic, the probe beam, supercontinuum, is of different frequency at different time in the sample. After pass through the object, a piece of glass sheet composed of four flat steps, the supercontinuum pulse was separated into four supercontinuum pulses with different delay time. Thus, the gating pulse, pump pulse, would interact with the different pulses at different frequency. That the OKG image would present different color for different glass thickness. With known chirp characteristic of the supercontinuum and given refractive index of the glass, the thickness or shape of the object can be obtained.

2.1.3 Using Echelon Mirrors

An echelon is an optic with plenty of stair steps (see Figure 2-5), which can subdivide the transverse profile of a probe beam into multiple distinct pulses, each with a different delay time and reach the sample at a different time. Thus they can sense the transient information induced by the pump beam at different delay time to implement single-shot measurement.

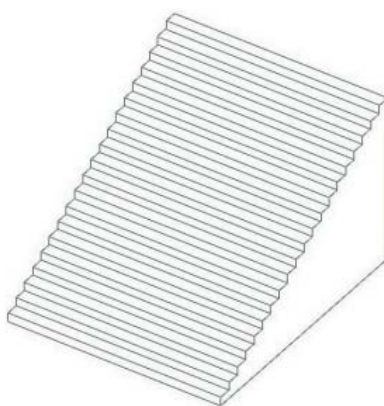


Figure 2-5: A draft of an echelon which is an optic with plenty of stair steps, which can subdivide the transverse profile of a probe beam into multiple distinct pulses, each with a different delay time and reach the sample at a different time.

In 2000, K A Nelson et al. of MIT first developed a femtosecond time-resolved single-shot pump-probe technique by introducing dual-echelon into the probe light path [111,112]. In Figure 2-6, it is the schematic of experimental setup. The crossed echelons subdivide a probe pulse into a pulse train with 25-fs time increments and covering a total temporal range of 10 ps. In 2006, they applied this technique to monitor in a single laser shot organic crystalline reaction dynamics despite the formation of permanent photoproducts that cannot be conveniently removed [113]. Then, this technique is widely used in diversified ultrafast single-shot real-time

measurements [114-117].

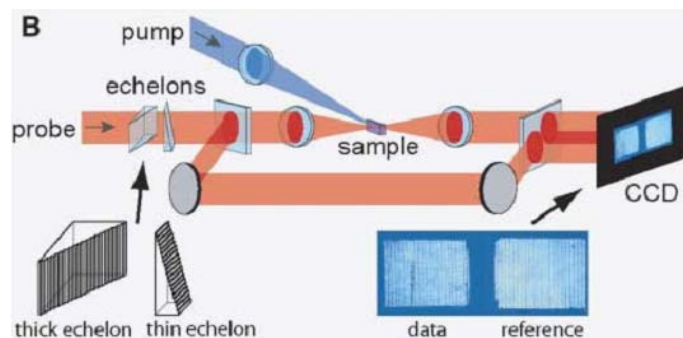


Figure 2-6: Schematic of dual-echelon single-shot femtosecond spectroscopy [113]

2.2 OKG Measurements

There are various kinds of pump-probe spectroscopy based on different transient physical effects, including absorption, fluorescence, four-wave-mixing, polarization rotation and so on. Here, the pump-probe spectroscopy we focus on is the OKG measurements based on optical Kerr effect (polarization rotation).

2.2.1 The principle of OKG measurements

As the name implies, OKG is based on optical Kerr effect. It is that intense laser beam induced change in the refractive index of a material. Figure 2-7 is a schematic of OKG setup. The OKG is made up of a Kerr medium and two crossed polarizers placed before and after the Kerr medium. Without the pump beam, the probe beam can not pass through the analyzer. OKG is off. And when the pump and probe beams pass through the medium at the same time and overlapped with each other, the pump beam will induce a birefringence of the Kerr medium, and the polarization of the probe beam will change from a lineally polarized light to an elliptically polarized light. Thus part of the probe beam can pass through the crossed analyzer and can be

detected. At this time, the OKG is open.

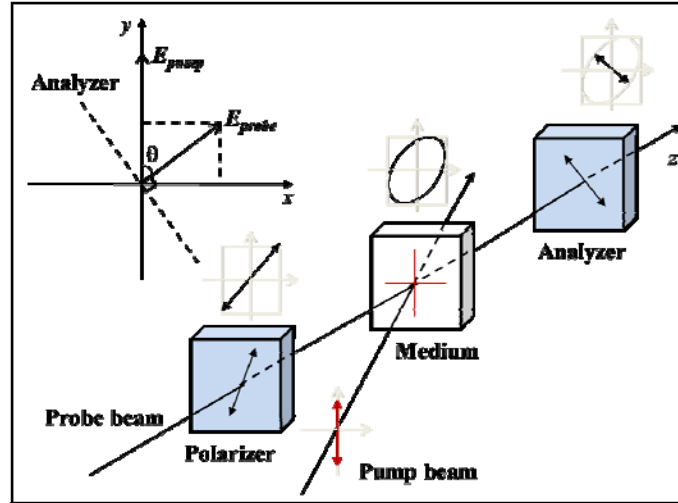


Figure 2-7: A schematic of OKG setup. The OKG is made up of a Kerr medium and two crossed polarizers placed before and after the Kerr medium. Without the pump beam, the probe beam can not pass through the analyzer. OKG is off. And when the pump and probe beams pass through the medium at the same time and overlapped with each other, the pump beam will induce a birefringence of the Kerr medium, and the polarization of the probe beam will change from a linealy polarized light to an elliptically polarized light. Thus part of the probe beam can pass through the crossed analyzer and can be detected. At this time, the OKG is open.

In the upper left corner of Figure 2-7, it is a vectogram of optical Kerr effect. Here the electric field vectors of the pump and pump beams are both lie in the xy -plane. The direction of of electric field vector of the pump beam, the direction of polarization of the pump beam, is in y -direction. The probe beam is polarized in the direction with a polarizing angle θ with the pump beam. After passing through the Kerr medium, the electric field of the probe beam can be described as

$$\begin{cases} E_x = E_{probe} \sin \theta \cos(\omega t) \\ E_y = E_{probe} \cos \theta \cos(\omega t + \Delta\phi) \end{cases} \quad (2-1)$$

Here, $\Delta\phi$ indicates the phase shift caused by the light-induced birefringence effect,

which is proportional to the pump intensity I_{pump} , can be written as [118]

$$\Delta\phi = \frac{2\pi}{\lambda_{probe}} n_2 L_{eff} I_{pump} \quad (2-2)$$

Here, n_2 is the optical Kerr nonlinear refractive index, L_{eff} is the effective medium length, λ_{probe} is the probe-beam wavelength.

Then, the probe beam transmitted through the analyzer, and the field components along the direction of the polarizing axis of the analyzer are

$$\begin{cases} E_{x-P_2} = -E_x \cos\theta = \frac{1}{2} \sin(2\theta) E_{probe} \cos(\omega t) \\ E_{y-P_2} = E_y \sin\theta = -\frac{1}{2} \sin(2\theta) E_{probe} \cos(\omega t + \Delta\phi) \end{cases} \quad (2-3)$$

Thus the electric field of the probe beam transmitted through the analyzer is

$$E_{P_2} = E_{x-P_2} + E_{y-P_2} = E_{probe} \sin(2\theta) \sin(\Delta\phi / 2) \sin(\omega t + \Delta\phi / 2) \quad (2-4)$$

And the intensity of the probe beam transmitted through the analyzer, the intensity of OKG signal, which is $I_{OKG} \propto E_{P_2} \cdot E_{P_2}^*$, can be given by

$$I_{OKG} = I_{probe} \sin^2(2\theta) \sin^2\left(\frac{\Delta\phi}{2}\right) \quad (2-5)$$

Here, I_{probe} is the intensity of the linearly polarized probe beam before passing through the Kerr medium. From Eq. (2-2) and Eq. (2-5), we can see the OKG signal intensity is dependent on the intensity of the pump and probe beams, and the polarization angle between the pump and probe beams. The polarization angle is usually set at 45° to get an optimum OKG signal. And the pump beam intensity is not the higher the better, however, when the phase shift is small, $\sin\left(\frac{\Delta\phi}{2}\right) \approx \frac{\Delta\phi}{2}$, the OKG can be

$$I_{OKS} \propto \left(\frac{\Delta\phi}{2} \right)^2 \propto I_{pump}^2 \quad (2-6)$$

That is, when the nonlinear phase shift is small (low pump intensity), the intensity of OKG signal is proportional to the square of the intensity of the pump beam [119-121].

Figure 2-8 shows the Kerr efficiency of quartz and SFL-6 dependence of the gate intensity [122]. We can see the Kerr efficiency increases with increasing gate intensity (pump intensity).

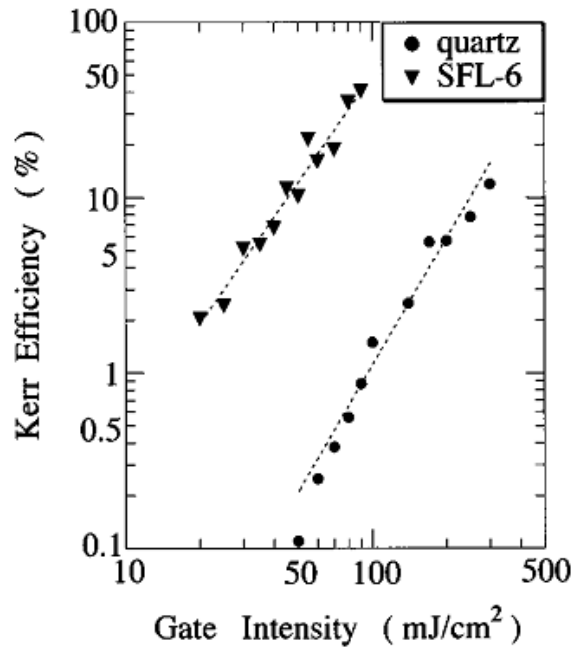


Figure 2-8: Kerr efficiency of quartz and SFL-6 dependence of the gate intensity [122]

2.2.2 FTOP Technique

The OKG technique has been developed about half a century since it was first proposed in 1969. For the last few decades, femtosecond OKG technique has been developed as one of the most effective methods for ultrafast phenomenon detection. This technique could provide an ultrafast measurement of high time resolution (~ 100

fs), high signal-to-noise ratio, and without the need for phase matching. Hence, it has been widely used in various ultrafast measurements, such as measurement of the third-order nonlinear response of all kinds of materials, ultrafast fluorescence spectroscopy, ballistic optical imaging, simultaneous three-dimensional (3-D) imaging, etc.

FTOP based on OKG, can be used to directly observe the instantaneous intensity distributions of ultra-short pulses propagating in transparent mediums with two-dimensional spatial distribution. Figure 2-9 shows the schematic of FTOP. Compared with a general OKG, its specialty is the direction of propagation of the pump and probe beams are perpendicular with each other. Thus the probe beam could sense two-dimensional profile of the propagating pump pulse. The single-headed arrows indicate the propagation directions of the pump and probe pulses. The double-headed arrows indicate the polarization direction of the pulses which are both linearly polarized. According to the optical Kerr effect, when the intense femtosecond laser pulse propagating in the medium, it would induce anisotropic change of refractive index in the medium in proportion to its intensity distribution. The probe beam would sense the birefringence and its polarization state would be changed. Thus part of the probe beam would pass through the analyzer and can be detected. The detected probe beam intensity can reflect the instantaneous intensity distribution of the intense femtosecond laser pulse.

As shown in Figure 2-9, the polarization directions of the pump and probe beams change in the yz -plane and xy -plane, respectively. θ is the angle between the polarization direction of the probe beam and the y -axis. When the pump beam is polarized in the y -direction, the polarization angle between the pump and probe beams is θ .

described in Eq. (2-5). Thus, an optimum OKG signal would be obtained when θ equals 45° as shown in Figure 2-9.

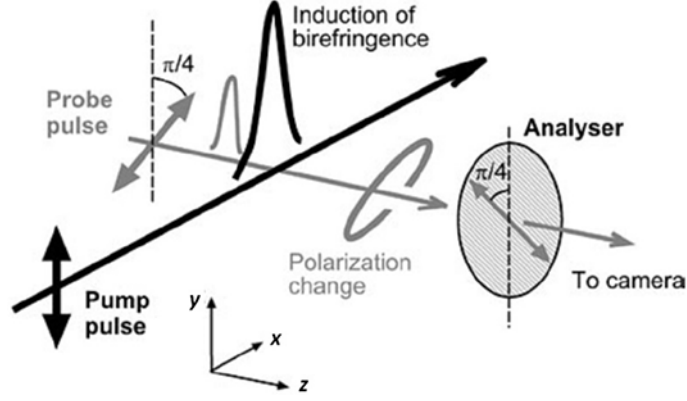


Figure 2-9: The schematic of FTOP. The single-headed arrows indicate the propagation directions of the pump and probe pulses. The double-headed arrows indicate the polarization direction of the pulses which are both linearly polarized. According to the optical Kerr effect, when the intense femtosecond laser pulse propagating in the medium, it would induce anisotropic change of refractive index in the medium in proportion to its intensity distribution [47].

If the polarization direction of the pump beam is not in the y-direction, it is necessary to suppose α is the angle between the polarization direction of the pump beam and y-axis. Thus the nonlinear refractive index changes in x- and y-direction induced by the electric field components of the pump beam in y- and z-direction are

$$\begin{cases} \Delta n_{yx} = \frac{3k_0}{k} \chi_{xyyy}^{(3)}(\omega; \omega, \omega', -\omega') |E(\omega') \cos \alpha|^2 \\ \Delta n_{yy} = \frac{3k_0}{k} \chi_{yyyy}^{(3)}(\omega; \omega, \omega', -\omega') |E(\omega') \cos \alpha|^2 \end{cases} \quad (2-7)$$

$$\begin{cases} \Delta n_{zx} = \frac{3k_0}{k} \chi_{xxzz}^{(3)}(\omega; \omega, \omega', -\omega') |E(\omega') \sin \alpha|^2 \\ \Delta n_{zy} = \frac{3k_0}{k} \chi_{yyzz}^{(3)}(\omega; \omega, \omega', -\omega') |E(\omega') \sin \alpha|^2 \end{cases} \quad (2-8)$$

Thus, the refractive index changes in x- and y-direction are Δn_x and Δn_y , which can

be written as $\Delta n_x = \Delta n_{yx} + \Delta n_{zx}$, $\Delta n_y = \Delta n_{yy} + \Delta n_{zy}$. And the corresponding phase shift between x- and y-direction is

$$\Delta\phi = \frac{2\pi}{\lambda_{probe}} (\Delta n_y - \Delta n_x) L_{eff} = \frac{6\pi L_{eff}}{\lambda_{probe} n} (\chi_{yyyy}^{(3)} - \chi_{xxyy}^{(3)}) |E(\omega') \cos \alpha|^2 \quad (2-9)$$

From Eq. (2-9) we can see when α equals 0° , the pump beam polarized in y-direction, the phase shift will reach an optimum value, and the FTOP signal intensity can be described as the general OKG signal intensity

$$I_{FTOP} = I_{probe} \sin^2(2\theta) \sin^2\left(\frac{\Delta\phi}{2}\right) \quad (2-10)$$

Notice that here θ is the angle between the polarization direction of the probe beam and y-direction, is determined by Eq. (2-9) which is tied to the angle α .

2.3 Summary

The pump-probe spectroscopy is one of the most effective way to study ultrafast dynamic processes. However, the traditional pump-probe spectroscopy can not fullfill single-shot measurement which is not suitable for irreversible ultrafast dynamics. Single-shot pump-probe spectroscopy based on supercontinuum, is a time- and frequency-resolved technique using a supercontinuum with chirp characteristic induced by ultrashort laser pulses in transparent medium as the probe beam. Because of chirp characteristic, the supercontinuum components of different wavelength is of different delay time, thus they could sense the transient information in the sample at different delay time in a single shot. Therefore, it does apply to the measurements of ultrafast dynamic processes. An echelon is an optic with plenty of stair steps which can subdivide the transverse profile of the probe beam into multiple distinct pulses, each with a different delay time and reach the sample at a different time. Thus they

can sense the transient information induced by the pump beam at different delay time to implement single-shot measurement.

The OKG measurement, one of pump-probe spectroscopy, based on optical Kerr effect, has been developed as one of the most effective methods for ultrafast phenomenon detection. FTOP based on OKG, can be used to directly observe the instantaneous intensity distributions of ultra-short pulses propagating in transparent mediums. However, the traditional FTOP method can hardly obtain the whole map of a single pulse's propagation instantaneously. Therefore, it is necessary to develop single-shot pump-probe techniques, which can also be used for single-shot imaging of ultrashort pulses propagation.

Chapter 3

Ultrafast Single-Shot Imaging of Femtosecond Pulse Propagation in Transparent Liquids Using FTOP and a Supercontinuum

3.1 Introduction

The advent of femtosecond laser necessitates the research of the propagation characteristic of ultrashort and intense laser pulses, which involves various self-modulating nonlinear effects. And the propagation mode of laser filamentation has aroused a great interest due to its numerous potential applications, such as atmospheric analysis, power supply for high speed electric vehicles, and generation of terahertz radiation. In the past few years, various methods have been developed to research the propagation behaviors of intense laser pulses in transparent media, like holography, shadow-imaging, three-dimensional imaging, etc. FTOP, one of OKG measurements, is a direct method for observing the pulse propagation of a focused femtosecond laser. This method based on optical Kerr effect uses the instantaneous birefringence induced by the strong electrical field of the pulse in transparent

materials. Through consecutive femtosecond snapshot images of intense femtosecond laser pulses propagating in the medium, ultrafast temporal changes in the two-dimensional spatial distribution of the optical pulse intensity can be observed. However, the traditional FTOP method can hardly obtain the whole map of a single pulse's propagation instantaneously, as amount of snapshot images are needed to be stacked to display the whole image. Because these images are taken using a serial of independent pulses, it cannot fulfill the single-shot measurements of the spatial propagation distribution of an intense light pulse, while single-shot technique is especially important for the research of irreversible effect of the intense pulse with the propagation medium. In 2002, Fujimoto et al. demonstrated a successive four-frame instantaneous observation of an intense femtosecond optical pulse propagating in air [123]. However, a quadruple-pulse generator installed in the optical path is needed in the experiments. This will largely increase the difficulty and complexity of the experiments. Therefore, it is necessary to develop single-shot pump-probe techniques, which can also be used for single-shot imaging of ultrashort pulses propagation.

In this paper, we have performed the single-shot imaging of femtosecond laser pulses propagating in N-methyl-2-pyrrolidone (NMP) and CS₂, respectively, using FTOP and a supercontinuum. Because of the chirp character of the supercontinuum, the wavelength distributions of the FTOP images can agree well with the pulse propagation time. The spectral widths at fixed position of CS₂ are broader than in NMP due to its slow time response. Through image analysis using Hue-Saturation-Value (HSV) model, it is found that the saturation in CS₂ is lower than in NMP on account of mixing of more colour component at every corresponding position.

3.2 Experimental methods

In our experiments, we selected two transparent liquids of NMP and CS₂ as the Kerr media. Firstly, the nonlinear responses of the two samples were measured using time-resolved optical Kerr gate (OKG) method. It was performed using 65 fs, 800 nm pulses from a regeneratively amplified Ti: sapphire laser system (Libra-USP-HE, Coherent Inc.) operating at 1 kHz repetition rate with horizontally linear polarization. The measurement setup used was similar to that reported elsewhere [124]. Figure 3-1 shows the time-resolved OKG signals of the samples. The red circles and the black squares in Figure 3-1 refer to the OKG signals of NMP and CS₂, respectively. The red solid curve indicates the Gaussian fit of OKG signals of NMP, the full-width at half-maximum (FWHM) of which is about 120 fs. As the OKG signals for NMP show no obvious slow decay process, the origin of the nonlinear response of NMP could be

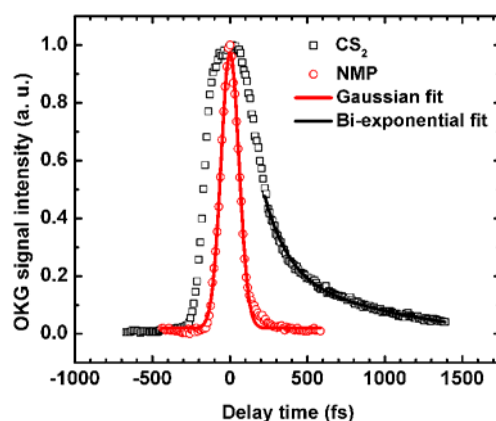


Figure 3-1: Time-resolved measurements of OKG signals for NMP and CS₂. The red circles and the black squares are the experimental data of NMP and CS₂, respectively. The red solid curve indicates the Gaussian fit of NMP. The black curve of CS₂ is fitted by a bi-exponential decay function with time constants 160 fs and 1.6 ps.

mainly attributed to electronic process, the characteristic time of which is much faster

than 120 fs. The black curve in Figure 3-1 indicates the decay process of the nonlinear response of CS₂, which is fitted using a bi-exponential decay function with time constants 160 fs and 1.6 ps. The fitted result agrees well with those reported in the previous research, indicating that the slow decay process of nonlinear response in CS₂ should be mainly attributed to molecular orientation relaxation [125].

Then, we performed the single-shot imaging of femtosecond laser pulses propagating in NMP and CS₂ using FTOP and a supercontinuum. The general scheme of the experiment is shown in Figure 3-2. The laser beam was split into a pump and a probe beam by a beam splitter. After passing through a delay line, the polarization of the pump beam was changed to vertical using a half-wave plate. The pump beam was focused into a 10-mm long fused silica cuvette filled with sample (NMP or CS₂) by a 100 mm lens. The nonlinear focus of the pump beam was located at about 1 mm inside the input window of the cuvette. The probe beam was focused into a 10 mm cell filled with distilled water to generate a supercontinuum by a 100 mm lens. Through nonlinear interactions including self-phase modulation, self-steepening, stimulated Raman scattering, and four-wave mixing, the broad supercontinuum was produced extending down to 450 nm [128]. To temporally broaden the supercontinuum pulse, a 20-mm thick fused silica was introduced into the optical path of the probe beam. The supercontinuum, after passing a short-wave-pass filter to remove the 800 nm light and the infrared part, was collimated and introduced into the sample cell perpendicularly to the direction of the pump path. The light spot of the supercontinuum covered the area of the focal point of the pump beam. In front of the sample, a polarizer (P1) was set to 45° with respect to the horizontal plane of the optical stage and allowed parts of the supercontinuum to pass. When the pulse passed

through the interaction region, only the components perpendicular to the polarizer could be extracted by the analyzer (P2) placed behind the sample. To record the FTOP image, a high-spatial-resolution CCD camera was located on the imaging plane of the filaments.

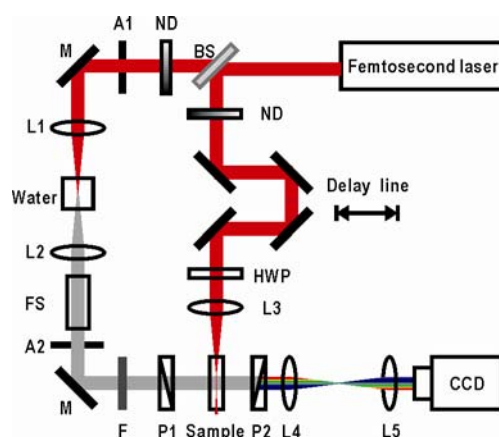


Figure 3-2: Experimental setup for FTOP, where a supercontinuum generated in water was used as the probe light. BS: beam splitter, M: mirror, ND: neutral density filter, A: aperture, L: lens, FS: fused silica, F: short-wave pass filter, P: polarizer, and HWP: half-wave plate.

3.3 Results and discussion

The recorded FTOP images of the pump pulse propagation in NMP and CS₂ are shown in Figure 3-3(a) and (b), respectively. To increase the signal-to-noise ratio, the pump powers were fixed at 44.5 mW in NMP and 11.5 mW in CS₂, and the exposure times during the measurements in the samples were set to be 1/6 s in NMP and 1/75 s in CS₂. The laser pulse traveled from left to right. Due to the chirp character of the supercontinuum, different wavelength components overlapped with the pump pulse at different propagating time in samples. The colours of recorded images change from red to blue, while different colour corresponds to different time of the pulse propagating in the medium. Because of the balance between Kerr self-focusing and

plasma defocusing induced by the nonlinear ionization, a filament was produced in a sample. The recorded filaments last about 3 mm long in samples.

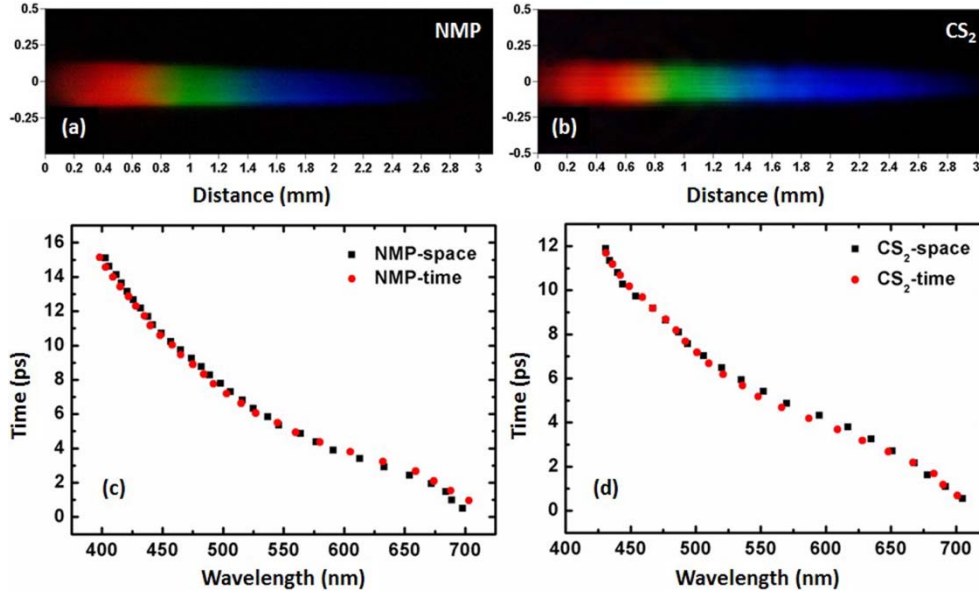


Figure 3-3: Imaged filaments induced by a femtosecond laser pulse in (a) NMP and (b) CS₂, the CCD exposure times are 1/6 s and 1/75 s, respectively. Distance means the propagation distance of the pump pulse in the irradiated range of the supercontinuum. Chirp character of the supercontinuum (red circles) and wavelength distributions of the recorded images (black squares) in (c) NMP and (d) CS₂.

Then, we analyzed the relation between the chirp character of supercontinuum and the spatial spectra distribution of FTOP images. The chirp character of the supercontinuum was measured using a general OKG measurement. The red circles in Figure 3-3(c) and (d) indicate the temporal distributions for different wavelength components of the supercontinuum. The spatial spectra distributions of the FTOP images were obtained by finely moving the fiber optic spectrometer along the pulse propagation direction behind the analyzer (P2). The fiber diameter is about 100 μm . For comparison, we converted the propagation distance of the 800-nm pulse to the

propagation time in the samples. Here, the linear refractive indexes of 1.62 for CS₂ and 1.47 for NMP at 800 nm were used. In Figure 3-3(c) and (d), the black squares indicate the spatial spectra distributions of the FTOP images, which accord well with the chirp character of the supercontinuum measured beforehand. Therefore, by selecting a wavelength at a certain distance from the recorded image, one can finely determine the propagation time of a pulse in an indeterminate medium, as well as the spatial intensity distribution at the corresponding time by referencing the chirp character of the supercontinuum.

Furthermore, we compared the difference of the FTOP images recorded in NMP and CS₂, which showed fast and slow responses, respectively. Figure 3-3(a) and (b) we can see that, the colour of the recorded FTOP image in NMP, is purer than that in CS₂. To explain this phenomenon, we measured the spectra of the FTOP images at different positions by moving the fiber optic spectrometer behind the analyzer (P2) along the pulse propagation direction. In Figure 3-4, the red line and the black line indicate the spectral lines of NMP and CS₂, respectively, where the central wavelengths were fixed at 450 nm, 500 nm, 550 nm and 600 nm. Because CS₂ has a much longer response time than NMP, a residual birefringence would be experienced by the following arrived spectral components of the probe supercontinuum. Hence the recorded spectra in the detecting region should be wider in CS₂ than those in NMP. In our experiments, however, the spectra of the FTOP signal were coupled into the spectroscopy using a fiber with a 100 μm diameter. In the collecting region of 100 μm, the propagation time of the pump pulse was estimated to be about 500 fs in the samples, which was much longer than the response time of NMP and comparable to the FWHM of the OKG signals of CS₂. Hence, the spectra difference was not as

remarkable as the difference of the response time of the two samples.

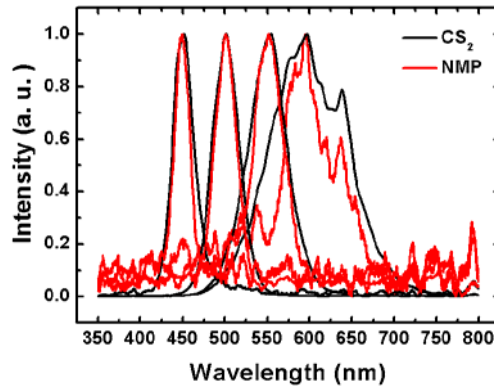


Figure 3-4: The spectra of the FTOP images along the pulse propagation direction detected by fiber optic spectrometer behind the analyzer (P2).

For further understanding, we used HSV colour model to analyze the recorded images as shown in Figure 3-5. HSV stands for hue, saturation, and value. Hue scales the perceived colors: red, yellow, green, and blue, or to a combination of two of them. Saturation is a ratio of chroma to the maximum chroma of a colour, which indicates the chromatic purity. Value, also often called brightness, is defined as the location of a visual perception along a continuum from black to white. In Figure 3-5, the red line and black line show the saturation curves of the FTOP images in NMP and CS₂, respectively. The horizontal axis indicates the propagation distance of the laser pulse, which is consistent with that in Figure 3-3. The corresponding hue curves of the images are presented in the inset of Figure 3-5, which showed almost the same variation tendency. The saturation of the FTOP image in NMP is higher than that in CS₂, indicating that the colour purity of the FTOP image in NMP is much higher. Due to the slow response of CS₂, a residual birefringence would be left when the pump pulse passed through a fixed position in the sample. Thus, more wavelength components of the probe light would be effected and pass through the analyzer,

resulting the chromatic impurity of the FTOP image. In addition, the colours of the FTOP images change rapidly from the propagation distance 0.5 to 1.2 mm, as indicated by the hue curves shown in the inset of Figure 3-5. Therefore, different wavelength components were mixed more easily in the FTOP image of CS₂ due to its slow response, and a vast gap in the vicinity of 0.8 mm between the saturation curves was observed.

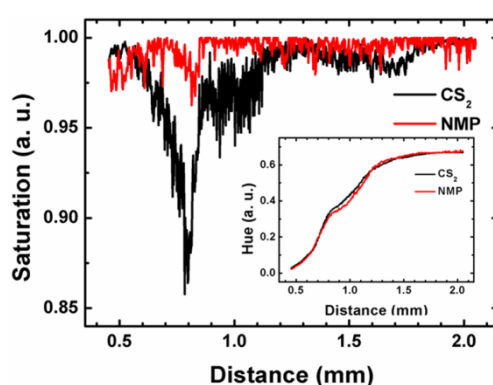


Figure 3-5: The saturation of the FTOP images along the pulse propagation direction. The inset shows the corresponding hue of the images.

3.4 Summary

In this chapter, we have investigated the ultrafast time-resolved single-shot imaging of femtosecond filaments using supercontinuum and FTOP method in NMP and CS₂. The wavelength distributions of the FTOP images corresponded with the pulse propagation time because of the chirp character of the supercontinuum. In the slow time response sample CS₂, the spectral widths at fixed position were broader than those in the fast time response sample NMP. It was because in the slow response sample, the probe light experienced the residual birefringence of pump light. Thus, the FTOP image contained more wavelength components at every position along the

pump pulse propagation direction in the slow time response sample, and the FTOP image in the fast time response sample was with higher saturation values.

Chapter 4

High-Frame-Rate Observation of Single Femtosecond Laser Pulse Propagation in Fused Silica Using FTOP and an Echelon

4.1 Introduction

Since the intense laser pulses develop complex structures during their propagation arising from self-modulation due to nonlinear effects, the propagation profile is quite different from shot to shot, even if the laser light source fluctuates slightly. As the traditional FTOP method is conventionally conducted with a pump pulse and a variably delayed probe pulse, with many repetitions of the pump-probe sequence, it's difficult to observe the instantaneous intensity distributions of a single laser pulse at several successive temporal points.

To fulfill the single-shot detection of the intense laser pulse propagation, M. Fujimoto et al installed a quadruple-pulse generator in the optical path and realized a successive four-frame instantaneous observation of an intense pulse propagating in air [123]. However, the quadruple-pulse generator which combines four different probe

beams with different optical paths will largely increase the complexity of the experiments. Some other single-shot imaging technique, such as tomography [131,132] and x-ray diffraction [133,134] methods have been proposed to visualize ultrafast phenomena. For example, N. H. Matlis et al observed the structure and position information for laser-induced plasma filaments using a single-shot ultrafast tomographic imaging by spectral multiplexing [131].

In this paper, we demonstrate a simple multi-frame observation method of femtosecond laser pulse propagating in transparent medium based on FTOP and an echelon. A stair-step echelon was introduced into the probe light and divided it into multi-pulse both in time and space, allowing a multi-frame detection of the intense laser pulse propagating in materials. Using this method, we realized a four-frame observation of a single femtosecond laser pulse propagating in fused silica. As the material had an ultrafast nonlinear response, the temporal resolution of the imaging in fused silica was mainly limited by the pulse duration, and the frame rate of the imaging could be higher than 1 THz. The influence of pulse-energy fluctuation on the spatial and temporal distribution of the single laser pulse was visualized using the single-shot measurements.

4.2 Experimental methods

Figure 4-1 illustrates the experimental setup. The experiments were performed using 65 fs, 800 nm pulses from a regeneratively amplified Ti: sapphire laser system (Libra-USP-HE, Coherent Inc.) operating at 1 kHz repetition rate. The laser beam was split into a pump and a probe beam by a beam splitter. After passing through a delay line, the polarization of the pump beam was changed to vertical using a half-wave

plate. The pump beam was focused into a 10-mm long Kerr medium of fused silica glass by a lens of 100-mm focal length. The nonlinear focus of the pump beam was located at about 1 mm inside the input surface of the samples. To avoid the background scattering of the pump light, the probe beam was frequency doubled to 400 nm by a 1-mm thick β -barium borate (BBO) crystal. Then it was collimated by a confocal lens and passed through a stair-step echelon, see Figure 4-2 for details, which separated the probe light in space and time. The modulated probe light was then introduced into the Kerr medium perpendicularly to the direction of the pump path, with the light spot covering the area of the focal point of the pump beam. In front of fused silica, a polarizer (P1) was set to 45 degree with respect to the horizontal plane of the optical stage and allowed parts of the probe light to pass. When the pulse passed through the interaction region, only the components perpendicular to the polarizer could be extracted by the analyzer (P2) placed behind the sample. To record the FTOP image, a high-spatial-resolution charge coupled device (CCD) camera was located on the imaging plane of the pump light path.

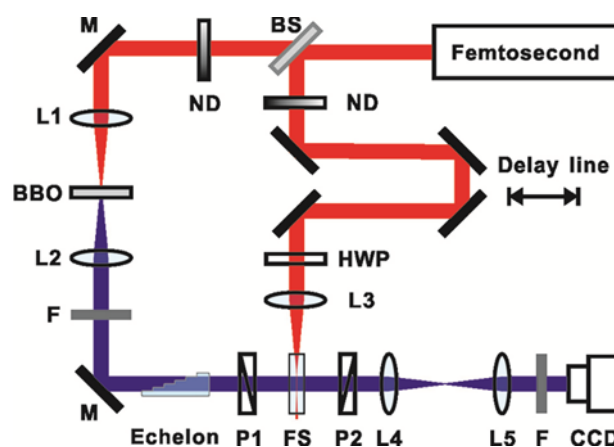


Figure 4-1: Experimental setup of multi-frame FTOP imaging technique using an echelon. BS: beam splitter, ND: neutral density filter, M: mirror, L: lens, FS: fused silica; P: polarizer, HWP: half-wave plate.

The echelon size with stair steps is confined by the experimental conditions, see Figure 4-2. Suppose every step of the echelon is with width of L and height of H , the refractive index of the echelon for the probe beam is n_1 , and the refractive index of the Kerr medium for the pump beam is n_2 . Thus the delay time between adjacent step is

$$\Delta t = (n_1 - 1)L / c \quad (4-1)$$

This delay time corresponds to the propagation distance of the pump beam in the Kerr medium, which is the height of the step,

$$H = \Delta t \cdot c / n_2 \quad (4-2)$$

Thus, the relationship between the step width and height of the echelon is

$$H = (n_1 - 1)L / n_2 \quad (4-3)$$

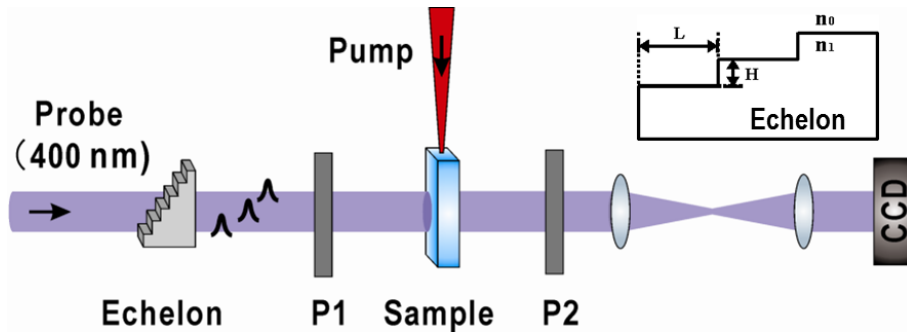


Figure 4-2: Schematic of FTOP using an echelon, in the upper right corner is a side view of steps of an echelon.

In our experiments, the echelon with 4 steps is mechanically fabricated on a microscope cover glass. The step width is about 0.54 mm, producing a time delay of about 0.96 ps for 400 nm probe pulse ($n=1.53$). As each step produces one frame of the FTOP image, the introduced delay time by each step must agree with the propagation time of the 800 nm pump pulse in fused silica ($n=1.45$). Hence, the height

of the step is designed to be about 0.20 mm ($\approx 0.96 \text{ ps} \times (c/1.45)$, $c=3.0 \times 10^8 \text{ m/s}$).

4.3 Results and Discussions

Figure 4-3 shows the recorded four-frame instantaneous FTOP image of 15 μJ pump pulse propagating in fused silica. The pulse propagated from the left to right. The exposure time of the CCD camera was set at 100 ms and 100 pulses were used to produce the image. The spatial resolution of the image is estimated to be 4.3 μm . The image has four profiles, each corresponding to one frame of the temporal intensity distributions of the laser pulse propagating in fused silica at different time. The interval between the peaks of adjacent profiles was 0.96 ps in time, correspondingly 0.2 mm in space, which was decided by the step width of the echelon. As each stair of the echelon had different thickness and transmittance, and the probe pulse intensity distribution was not strictly uniform, each frame of the FTOP image was normalized by comparing with the intensity distribution of the incident probe pulse after passing through the echelon. From the figure we can see that, the lateral size of the pump light

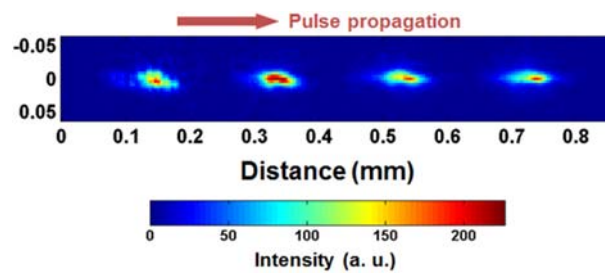


Figure 4-3: Four-frame observation of pulse propagation in fused silica using 100 pulses of 15 μJ . The pulse propagated from left to right.

spot changed slightly inside the sample even after the lens focus locating at 1 mm inside the sample. Because of the balance between Kerr self-focusing and plasma defocusing effect induced by the nonlinear ionization, a filament was produced inside

fused silica.

In the FTOP measurements, the probe pulse collides with the pump pulse while running through each other in the medium. If the radius of the pump beam and the nonlinear response of the material are finite, the temporal resolution of the imaging is determined only by the convolution of the probe pulse and the square of the integral of the intensity of the pump pulse [135]. For further analysis, we acquired the exposure intensity distribution along the propagating axis of the FTOP profiles given in Figure 4-3. The squares in Figure 4-4 show the acquired intensity distributions as a function of the propagating time of pump pulse. The red solid curves indicate Gaussian fits of the image intensity for each frame with the full-width at half-maximum (FWHM) of 276 fs. This value is absolutely larger than the FWHM of the convolution of the probe pulse and the square of the pump light intensity. In our experiments, the origin of the nonlinear response of the material is mainly attributed to electronic process, the characteristic time of which is much faster than the pulse duration. Hence, the influence of the nonlinear response of the material on the temporal resolution of the imaging could be neglected. The measured pump beam diameter is estimated to be about 40 μm . By considering the linear refractive index of the material, the interacting time of the pump and probe pulses is elongated by about 190 fs. Hence, the temporal resolution of the imaging is limited by the pulse duration and the lateral size of the pump beam in the sample. This also indicates that the echelon step size is limited by these factors.

The frame interval was estimated to be about 0.96 ps, corresponding to a frame rate of about 1.05 THz. It is much higher than 0.25 THz frame rate in CS_2 which we have obtained in previous work [136]. It should be noted that, the intensity of the

image after the second frame became lower as shown by Figure 4 2 and Figure 4 3. This was caused by the pump pulse energy reduction: because of the self-focusing effect of the pump beam during the filamentation process in fused silica, the pump beam intensity increases and might reach a certain value while propagating at a certain place, and then the pump pulse energy might reduce sharply by multiphoton absorption, or be refracted by ionization-induced refraction [31].

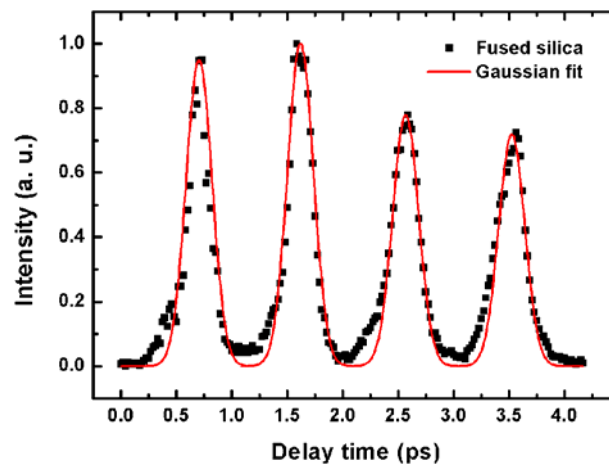


Figure 4-4: Exposure intensity distribution of the four-frame FTOP image as a function of the propagation time of the pump pulse. The solid lines show the Gaussian fit curves.

Then, we observed the propagation dynamics of a single laser pulse in fused silica in Figure 4-5(a). The CCD exposure time was set to 1 ms enabling single shot recording. The pump pulse energy was increased to 45 μJ to enhance the signal-to-noise ratio of the imaging. Similarly to Figure 4-4, the interval between the two adjacent profiles of the image was fixed at 0.2 mm. Propagation profiles under the same experimental conditions but for different laser shots are shown in Figure 4-5(b)-(d). These profiles are different from each other, which might be resulted from the pulse-energy fluctuation. For example, the intensity of Figure 4-5(a) is much higher than the other three. Meanwhile, the spatial and temporal positions of the most

intense part of each pulse propagating in the fused silica are also different from shot to shot due to the pulse energy distribution fluctuation at incidence.

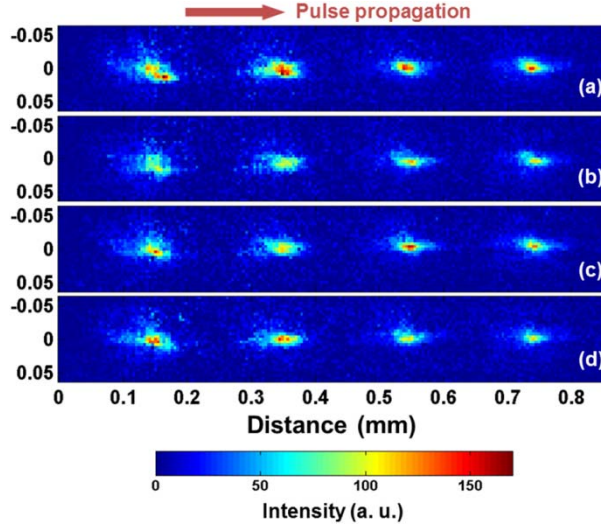


Figure 4-5: Single-shot four-frame observation of single 45 μJ pulse propagation in fused silica. The pulse propagated from left to right. (a)-(d) correspond to different laser shots under the same conditions.

Furthermore, we analyzed the intensity distributions of the single-shot images of the first frames shown in Figure 4-5(a)-(d). Figure 4-6A shows the intensity distributions of the images along the pulse propagation direction. From the figure we can see that, the peak intensity of the pulse fluctuates from shot to shot. Compared with the maximum peak in (a), the peak intensity of (b) is about 21% lower. The influence of the instability of the CCD exposure intensity could be ruled out, as the pulse-to-pulse energy stability of the pump pulse energy was measured to be 0.45% rms. Since the intense pump pulse might develop complex structures during their propagation arising from self-modulation due to nonlinear effects, the propagation profile is quite different from shot to shot, even if the laser light source fluctuates slightly. Figure 4-6B shows transverse intensity distributions of the corresponding

single pulse. It can be clearly seen that, transverse modes of the four pulses differ a lot from each other. Two peaks are observed in pulse (a) and (b), indicating that two filaments were formed when the pulse propagated in fused silica.

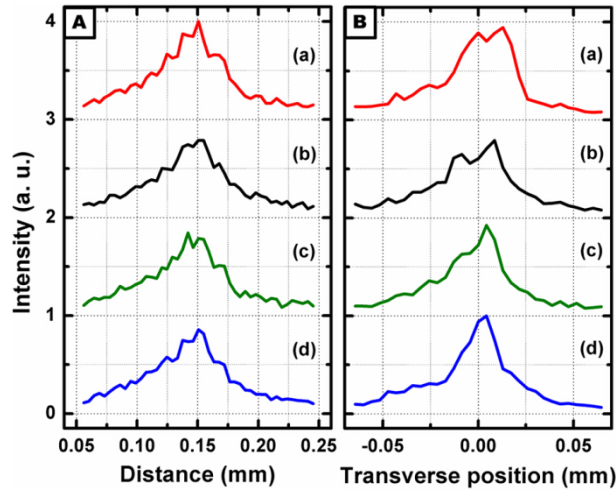


Figure 4-6: Intensity distributions of the first frames of the single-shot images shown in Figure 4-5(a)-(d). (A) Along the pulse propagation direction, and (B) along the transverse direction.

4.4 Summary

In this chapter, we have performed a successive four-frame instantaneous observation of single femtosecond laser pulse propagation in fused silica using an echelon combined with FTOP. Because of the ultrafast response of fused silica, the temporal resolution of the imaging is limited mainly by the probe pulse duration. The interval between adjacent frames is about 0.96 ps, corresponding to a frame rate of about 1.05 THz which is much higher than 0.25 THz obtained in our previous works in CS₂. From the single-shot images, we can directly observe the shot-to-shot variations of the pump pulse propagation profiles caused by the pulse-energy fluctuation.

Chapter 5

Pump Power Dependence of the Spatial Gating

Properties of Femtosecond OKG Measurements

5.1 Introduction

For the last few decades, femtosecond OKG technique has been developed as a key tool to measure the nonlinear response of all kinds of materials. This technique could provide an ultrafast measurement of broad wavelength range, ultrafast switching time, and high precision. Hence, it has been widely used in ultrafast imaging and microscopy areas, such as ballistic optical imaging, simultaneous three-dimensional (3-D) imaging, etc.

In the OKG measurements, an intense linearly polarized pump beam passing through the nonlinear material will cause the refractive index change of the sample. When the probe pulse overlaps with the pump beam temporally, a phase shift occurs between the probe field components polarized parallel and perpendicular to the polarization plane of the pump pulse. The OKG signal intensity is given by Eq. (2-5). In the previous reports, the OKG signals were considered quadratic dependence on pump power for the small phase shift and uniform in space[119]. In the OKG

measurements, however, when a pump beam with a nonuniform intensity distribution, such as a Gaussian mode was used, it might induce spatially nonuniform distribution of the phase change of the probe beam. If the pump is of high intensity, the transmittance of the OKG setup might vary sinusoidally as a function of pump power, and the OKG signals would present different spatial profiles depending on the pump intensity distribution. Hence, it's important to research on the spatial gating property of the OKG setup, especially when it is used in ultrafast imaging and microscopy areas.

In this paper, we investigated the evolution of spatial profiles of the femtosecond OKG signals as a function of pump power in CS₂. With the increase of pump power, the spatial pattern of the OKG signals changed from a Gaussian spot to a ring form, and then a spot surrounded by a concentric ring, successively. Furthermore, the OKG signal intensity at fixed position showed different pump power dependence with the spatially integrated OKG signal intensity. A series of numerical analysis was performed to explain the experimental results. Both the experimental and numerical results indicated that the spatial variation of OKG transmittance was attributed to the non-uniform spatially distributed refractive index change induced by pump beam with transverse mode of a Gaussian distribution.

5.2 Experimental methods

Figure 5-1 illustrates the experimental setup. The experiment was performed using 65 fs, 800 nm pulses from a regeneratively amplified Ti: sapphire laser system (Libra-USP-HE, Coherent Inc.) operating at 1 kHz repetition rate. The laser beam with a Gaussian intensity profile (TEM₀₀ mode) was split into two. The first one passing through a time-delay device was used as the pump beam. The other one which

was frequency doubled to 400 nm by a β -barium borate (BBO) crystal was used as the probe beam. The two beams were combined together by an unpolarized dichroic mirror (DM, with high reflective coating at 800 nm on one side and antireflective coating at 400 nm on the other side). Both of them were focused by a plano-convex lens (L3) with a focal length of 20 cm. A 2 mm thick quartz cell filled with CS₂ was placed 5 mm behind the focal point of the 800 nm pump beam. The pump beam radius in the sample was determined to be 190 μm at $1/e^2$, and the probe beam radius was enlarged about 5 times by the collimating lens (L2) behind BBO crystal, so that the probe intensity could be considered uniformly distributed compared with the pump. To avoid the white-light continuum generation, the pump energy was kept below 12 mW (about 0.01 J/cm²) [128]. A polarizer in a cross-Nicol configuration was placed behind the Kerr medium. To optimize the OKG signal intensity, the temporal overlap was maximized at zero time-delay, and the polarization plane of the pump pulse was rotated by 45° with respect to that of the probe pulse using a half-wave plate. The probe fluence distribution after the polarizer was recorded by a CCD camera with a 4f system. To block the 800 nm pump light, a bandpass filter centered at 400 nm was used in front of the CCD camera.

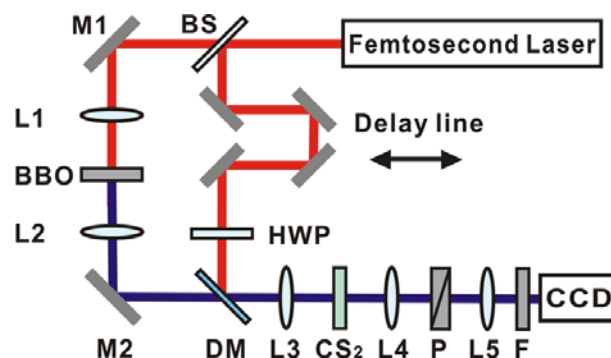


Figure 5-1: Scheme of the experimental setup. BS: beam splitter; DM: dichroic mirror; HWP: half-wave plate; P: polarizer; F: bandpass filter.

5.3 Results and discussion

In our work, 31 image data of the OKG signal profiles were collected with the pump power varying from 1.85 mW to 11.86 mW, and the corresponding pump fluence varying from 1.63 mJ/cm² to 10.46 mJ/cm². Figure 5-2(a)-(e) shows five typical recorded probe patterns of these OKG signals when the pump fluence was adjusted to 1.63 mJ/cm², 3.39 mJ/cm², 4.53 mJ/cm², 8.53 mJ/cm², and 10.46 mJ/cm², respectively. The color scales in all the pictures were adjusted to the same range. When the pump fluence was relatively low (see Figure 5-2(a)-(c)), the total intensity of the OKG signal grew with the increase of the pump fluence, and the pattern of each signal was a spot with Gaussian distribution. As the pump fluence increases higher, however, the OKG signal pattern changed to a ring form and then a spot surrounded by a concentric ring, as shown by Figure 5-2(d) and (e), respectively.

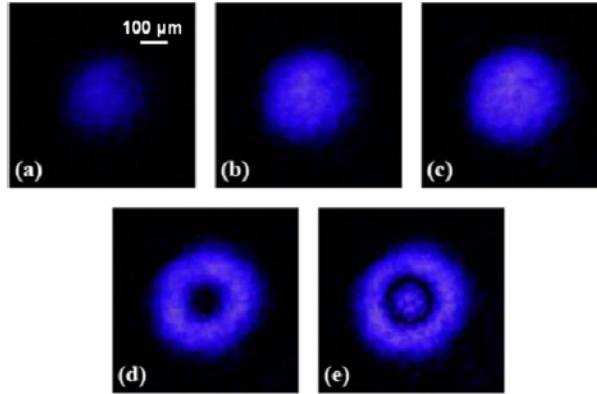


Figure 5-2: OKG signal profile when the pump fluence was fixed at (a) 1.63 mJ/cm², (b) 3.39 mJ/cm², (c) 4.53 mJ/cm², (d) 8.53 mJ/cm², and (e) 10.46 mJ/cm², respectively.

In our experiments, the pump beam with a Gaussian intensity distribution (TEM₀₀ mode) can be expressed by

$$I_{pump}(r) \propto F_{pump} e^{-2r^2/l_0^2} \quad (5-1)$$

Here, F_{pump} is the pump fluence, and r_0 is the radius of the Gaussian beam, which has been determined to be 190 μm . As the polarization angle between pump and probe beams, θ , is set at 45° , the spatial intensity of probe light with an uniform distribution passing through the polarizer behind the Kerr medium can be written as:

$$I_{OKG}(r) = A \sin^2(\Delta\phi(r)/2) = A \sin^2(BF_{pump} e^{-2r^2/r_0^2}) \quad (5-2)$$

Here, the term in the bracket denotes the phase shift $\Delta\phi(r)/2$ caused by birefringence effect. A and B are constants. The OKG signal intensity, $I_{OKG}(r)$, reaches the peak value of A when the phase shift $\Delta\phi(r)/2 = n\pi/2$ ($n = 1, 3, 5, \dots$), and reduces to the valley value of zero when $\Delta\phi(r)/2 = n\pi$ ($n = 0, 1, 2, \dots$). Since the laser transverse mode is of a Gaussian distribution, the phase shift of the probe, which is proportional to the pump intensity, decreases along the radial direction. Consequently, the transmittance of the OKG setup might present a spatially modulated intensity distribution when the pump fluence is increased.

To present the evolution of the OKG profiles more clearly, we acquired the one-dimensional exposure data along the horizontal radial direction from the collected images. The results corresponding to Figure 5-2 are shown by the discrete solid points in Figure 5-3(a)-(d). When the pump fluence was adjusted to 1.63 mJ/cm^2 and 3.39 mJ/cm^2 , the maximum value of phase shift $\Delta\phi(r=0)/2$ was smaller than $\pi/2$, and the OKG signals intensities were of Gaussian distribution as shown by Figure 5-3(a). With increasing pump fluence, the phase shift might be close to $\pi/2$ around $r=0$, and the OKG signals showed a top-flat profile as shown by Figure 5-3(b). In Figure 5-3(c), when the pump fluence was increased to 8.53 mJ/cm^2 , the phase shift $\Delta\phi(r)/2$ increased to about π around $r=0$, and decreased to $\pi/2$ at $r \approx \pm 120 \mu\text{m}$. Hence, the transmittance of the OKG setup presented a peak-valley-peak profile, and the OKG

signal pattern showed a ring form as shown by Figure 5-2(d). As the pump fluence increased to 10.46 mJ/cm^2 , the probe pulse experiences phase shift $\Delta\phi(r)/2$ as large as $\pi/2$ at $r \approx \pm 120 \text{ }\mu\text{m}$ and π at $r \approx \pm 60 \text{ }\mu\text{m}$, while reached to larger than π at around $r=0$. Therefore, the OKG pattern presented a central spot surrounded by a concentric ring, and the one-dimensional OKG signal distribution presented a multi-peak profile, as shown by Figure 5-2(e) and Figure 5-3(d), respectively.

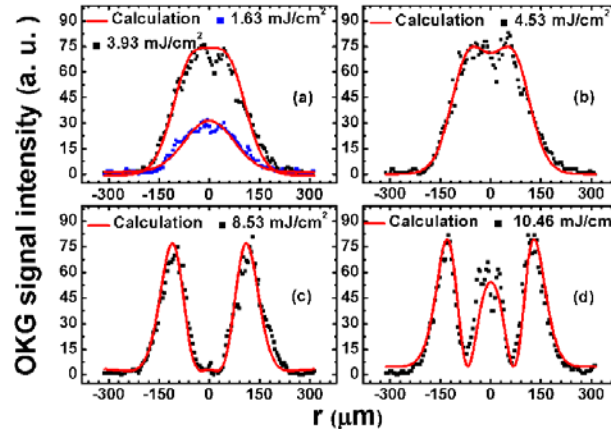


Figure 5-3: One-dimensional OKG signal intensity distributions when the pump fluence was fixed at (a) 1.63 mJ/cm^2 , (b) 3.39 mJ/cm^2 , (c) 4.53 mJ/cm^2 , (d) 8.53 mJ/cm^2 , and (e) 10.46 mJ/cm^2 , respectively. The discrete solid points are experimental results. The red solid lines indicate the calculated curves.

Using Eq. (5-2), we fitted the one-dimensional OKG signal intensity distributions at different pump fluence, and the parameters A, and B in Eq. (5-2) were calculated to be 75.00 and $0.394 \text{ cm}^2/\text{mJ}$, respectively. The red solid lines in Figure 5-3 indicate the calculated curves using Eq. (5-2) and the parameters obtained above. They accorded well with the experimental results as shown by the solid points, indicating that the spatial variation of the OKG transmittance was attributed to the transient non-uniform birefringence induced by pump beam with a Gaussian

distribution.

The squares in Figure 5-4(b) show the pump fluence dependence of OKG signal intensity at the fixed position of $r=0$. The red solid line in the figure indicates the calculated results using Eq. (5-2), which can be simplified to a sinusoidal function of the pump fluence when the value of r is fixed. The squares in Figure 5-4(a) indicate the spatially integrated intensity of the OKG signal profiles as a function of the pump fluence. By integrating Eq. (5-2), the spatially integrated OKG signal intensity can be expressed by:

$$\int I_{OKS}(r)ds = \int_0^{+\infty} A \sin^2 \left[BF_{pump} e^{-2r^2/r_0^2} \right] 2\pi r dr \quad (5-3)$$

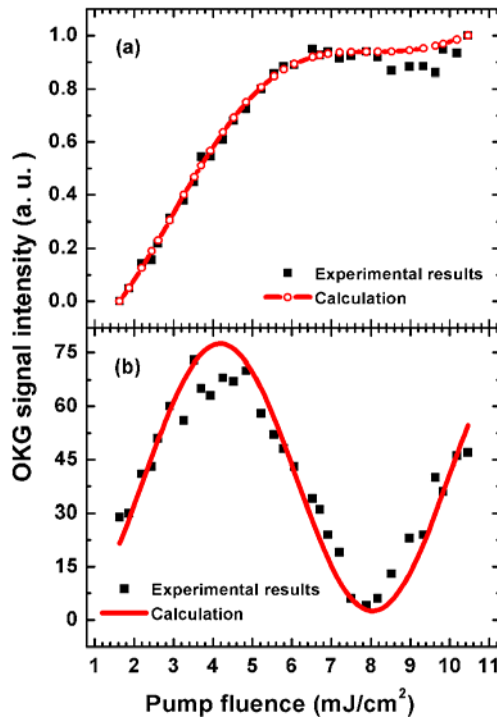


Figure 5-4: Pump fluence dependence of (a) spatially integrated exposure intensity of OKG signals and (b) OKG signals at $r=0$. The squares are experimental results. The red solid line indicates the calculated curves.

The red solid line with circles in Figure 5-4(a) shows the calculated results using

Eq. (5-3). Both the experimental results shown in Figure 5-4(a) and (b) accorded well with the calculated results. The integrated OKG signal intensity, however, showed different pump fluence dependence with OKG signal intensity at the fixed position. It increased sharply at low pump fluence, and then slowly when the pump fluence increased to be larger than 6 mJ/cm^2 . This difference could be attributed to the spatial variation of the OKG profiles due to the nonuniform spatially distributed phase change induced by the pump beam.

In addition, we measured the dependence of the OKG signal intensity on the polarization angle between the pump and probe beams to better understand the origin of the OKG signals. The squares and triangles in Figure 5-5 show the polarization dependence of the integral OKG signals, when the pump fluence fixed at 3.22 mJ/cm^2 and 10.30 mJ/cm^2 , respectively. In the experiments, we found the spatial patterns of the OKG signals remained the same at any polarization angle under the fixed pump fluence. So the phase shift of the probe is independent on the polarization angle. The solid line in Figure 5-5 shows the theoretical curve of the polarization dependence of the OKG signals using Eq. (5-1). The polarization dependence of the OKG signals showed a period of $\pi/2$, with the maximum and minimum values occurring at $n\pi/2 + \pi/4$ and $n\pi/2$ ($n = 0, 1, 2, \dots$), respectively. Hence, the OKG signals could be attributed to light-induced birefringence effect.

Finally, the spectra of the OKG signals at different pump fluence were measured, which showed the same structure with that of the incident probe light. Because the response time of CS_2 is more than 1 ps which is much slower than the probe pulse duration, the different wavelength components of the probe light experienced the uniform refractive index changes induced by the pump pulse. Hence, the spectral structure of the probe light passing through the OKG showed no obvious change.

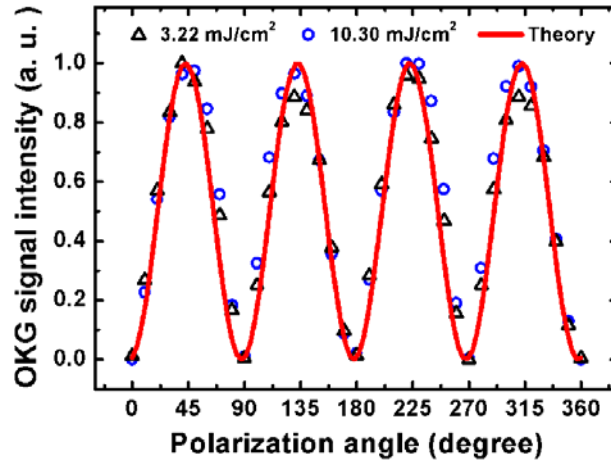


Figure 5-5: Polarization dependence of OKG signals, when the pump fluence was adjusted to 3.22 mJ/cm² and 10.30 mJ/cm², respectively. The squares and triangles are experimental results. The red solid line indicates the theoretical curve. The experimental results and the theoretical curve were both normal

5.4 Summary

In this chapter, we investigated the pump power dependence of the spatial gating properties of femtosecond optical Kerr effect measurements. When a pump beam with transverse mode of a Gaussian distribution was used in the femtosecond OKG measurements, it will cause a non-uniform spatially distributed refractive index change, and the spatial variation of OKG transmittance. With increasing pump power, the OKG signal intensity distribution changed from a Gaussian spot to a ring form, and then a spot surrounded by a concentric ring, successively. Furthermore, the OKG signal intensity at fixed position showed different pump power dependence with the spatially integrated OKG signal intensity, due to the non-uniform distributed refractive index change induced by the pump beam with a Gaussian mode.

Chapter 6

An Ultrafast OKG Measurement Based on Light-induced Polarization Ellipse Rotation

6.1 Introduction

In a traditional OKG, a powerful linearly polarized pump beam induces a transient birefringence in a Kerr medium, which results in a phase shift $\Delta\phi$ between the probe beam components polarized parallel and perpendicular to the polarization plane of the pump beam. After the linearly polarized probe beam passing through the Kerr medium, therefore, its polarization state changes and part of it can transmit through a crossed analyzer as OKG signal. The OKG signal intensity can be expressed by (2-5). We can see the OKG signal intensity is a function of the polarization angle θ which is usually set at 45° to get an optimum OKG signal. It means the OKG is gated by not only the pump beam intensity but also its polarization direction. When the pump beam is polarized parallel or perpendicular to the probe beam, the OKG is in a constant closed state. In addition, to avoid the optical Kerr effect induced by the probe beam, the probe beam intensity is usually set at very low level. Nevertheless, it is known that a circularly polarized light acting on an isotropic medium cannot induce any

anisotropy, and hence any induced birefringence [137].

Here, we proposed an OKG based on light-induced polarization ellipse rotation using an elliptically polarized probe beam, which can overcome the influence of the pump beam polarization direction and the probe beam intensity on the OKG signal intensity. Two crossed quarter-wave plates were introduced before and after the Kerr medium in a conventional OKG. Theoretical formula of this OKG was obtained, and it was verified by the experimental results. It was found that when the probe beam was a circularly polarized light, the OKG signal intensity would reach an optimum value and be independent of the pump beam polarization direction. And as a circularly polarized light, the birefringence induced by the probe beam which would influence the OKG signal intensity can be eliminated.

6.2 Experimental methods

The experimental setup is shown in Figure 6-1(a). The experiments were performed using 65-fs, 800-nm pulses from a regeneratively amplified Ti: sapphire laser system (Libra-USP-HE, Coherent Inc.) operating at 1 kHz repetition rate. The laser beam was split into pump and probe beams. Two $\lambda/2$ plates H1 and H2 were used to change the polarization angles of the linearly polarized input probe and pump beams after the polarizers P1 and P3, respectively. After passing through a delay line, the pump beam was focused into a 1-mm cell filled with CS₂ by a 20-cm lens (L3) where the pump beam induced a transient birefringence. The analyzer P2 was oriented for extinction of the probe beam in the absence of the pump beam, as a general Kerr gate. Here, we introduced a pair of crossed achromatic zero-order $\lambda/4$ plates before and after the Kerr medium in the probe beam path. The linearly polarized probe beam passed through the first $\lambda/4$ plate (Q1) to be an elliptically polarized light. Without the pump beam,

the second $\lambda/4$ plate (Q2) could exactly offset the phase shift caused by Q1, thus after Q2 the probe beam would return to its initial linearly polarization after H1 and be blocked by the analyzer P2. The OKG is “off”. With the pump beam, the optical Kerr effect (OKE) made the Kerr medium a transient birefringent crystal. Thus, when the elliptically polarized probe beam passed through the Kerr medium, polarization ellipse rotation would occur. Therefore Q2 could not offset the extra phase shift caused by OKE, enabling part of the probe beam passing through P2 to be detected by a photomultiplier tube (PMT). The OKG is “on”.

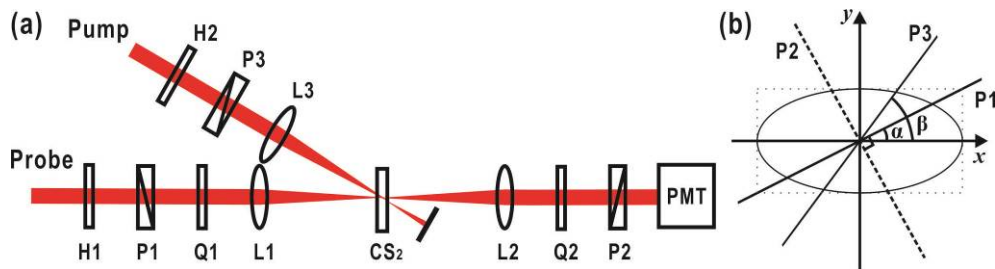


Figure 6-1: (a) Experimental arrangement for an OKG using an elliptically polarized probe beam.

P: polarizer; H: $\lambda/2$ plate; Q: $\lambda/4$ plate; L: lens; PMT: photomultiplier tube. (b) The geometry of the fields and the axes of the wave plates. x and y axes are fast and slow axes of Q1, respectively. E_{probe} is the probe field after H1 at angle α with respect to the fast axis of Q1. E_{pump} is the pump field after H2 at angle β with respect to the fast axis of Q1.

6.3 Theoretical calculations

Figure 6-1(b) shows the geometry of the pump and probe fields and the axes of the wave plates. x and y axes indicate the fast and slow axes of Q1, respectively. $\mathbf{E}_{\text{probe}}$ is the probe field after H1 at angle α with respect to the fast axis of Q1. \mathbf{E}_{pump} is the pump field after H2 at angle β with respect to the fast axis of Q1. Along the directions

parallel and perpendicular to the pump field, different refractive index changes Δn_{\parallel} and Δn_{\perp} ($\Delta n_{\parallel} > \Delta n_{\perp}$) are induced in the Kerr medium, respectively. The Kerr medium works as a transient birefringent crystal. This will give rise to a phase shift $\Delta\phi$, between the two polarization components parallel and perpendicular to the pump field, of a probe beam when it passes through the Kerr medium at this point. And this pump beam inducing birefringence can be considered equivalent to a wave plate, of which the slow axis is at β angle to the x-axis and the phase shift between the fast and slow axes is $\Delta\phi$. Therefore, the problem can be considered as a beam passing through a series of optical elements. Using Jones calculus, the probe field passing through H1 can be expressed as

$$\mathbf{E}_{p1} = E_0 \begin{pmatrix} \cos \alpha \\ \sin \alpha \end{pmatrix} \quad (6-1)$$

Here, E_0 is the amplitude of the probe field after H1. The Jones matrix of each optical element can be expressed as follows,

$$\begin{aligned} \mathbf{J}_{Q1} &= \begin{pmatrix} 1 & 0 \\ 0 & i \end{pmatrix}; \mathbf{J}_{Q2} = \begin{pmatrix} 1 & 0 \\ 0 & -i \end{pmatrix}; \mathbf{J}_{P2} = \begin{pmatrix} \sin^2 \alpha & -\sin(2\alpha)/2 \\ -\sin(2\alpha)/2 & \cos^2 \alpha \end{pmatrix}; \\ \mathbf{J}_G &= \cos(\Delta\phi/2) \begin{pmatrix} 1 + i \tan(\Delta\phi/2) \cos(2\beta) & i \tan(\Delta\phi/2) \sin(2\beta) \\ i \tan(\Delta\phi/2) \sin(2\beta) & 1 - i \tan(\Delta\phi/2) \cos(2\beta) \end{pmatrix} \end{aligned} \quad (6-2)$$

Here, J_{Q1} , J_{Q2} , J_{P2} , and J_G correspond to the Jones matrixes of Q1, Q2, P2, and Kerr medium, respectively. Thus the output light field is,

$$\mathbf{E}_t = \mathbf{J}_{P2} \mathbf{J}_{Q2} \mathbf{J}_G \mathbf{J}_{Q1} \mathbf{E}_{P1} = E_0 \sin(\Delta\phi/2) \begin{pmatrix} -\sin \alpha \sin(2\beta) + i \sin(2\alpha) \cos(2\beta) \\ \cos \alpha \sin(2\beta) - i \sin(2\alpha) \cos(2\beta) \end{pmatrix} \quad (6-3)$$

And the output light intensity is

$$I_{out} \propto \mathbf{E}_t^* \mathbf{E}_t = E_0^2 \sin^2(\Delta\phi/2) [1 - \cos^2(2\alpha) \cos^2(2\beta)] \quad (6-4)$$

Therefore, the theoretical formula of the OKG signal intensity based on light-induced nonlinear polarization ellipse rotation is,

$$I_{OKG-e} = I_{probe} \sin^2(\Delta\phi/2)[1 - \cos^2(2\alpha)\cos^2(2\beta)] \quad (6-5)$$

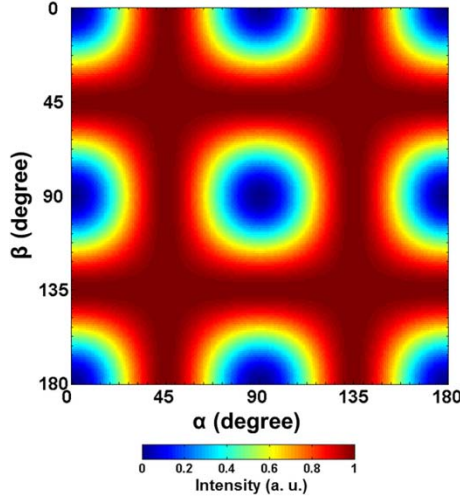


Figure 6-2: Theoretical calculation result of the OKG signal intensity based on light-induced polarization ellipse rotation using Eq. (6-5) .

Using Eq. (6-5), we get the theoretical simulation results of the OKG signal intensity dependence on α and β , as shown in Figure 6-2. The results are normalized.

We can see, when $\alpha=0$ (or $\alpha=\frac{\pi}{2}$), the probe light polarized along the fast (or slow) axis of Q1, thus after passing through Q1 the probe light is still a linearly polarized light. In this case, β (or $\frac{\pi}{2}-\beta$) indicates the polarization angle between the probe and pump beams in Eq. (2-5). Thus, Eq. (6-5) can be simplified to Eq. (2-5) as a general OKG. When $\alpha=\frac{\pi}{4}$, thus after passing through Q1 the probe beam changes to a circularly polarized light. At this time, the OKG signal intensity is independent of β , and reaches to the optimum value $I_{probe} \sin^2(\Delta\phi/2)$. It means when the probe light is a circularly polarized light, the OKG is only gated by the pump beam intensity. The OKG signal intensity is independent of the pump beam polarization direction, and

constant at the optimum value of a general OKG. Meanwhile, as a circularly polarized light, the birefringence induced by the probe beam can be eliminated.

6.4 Experimental results and discussion

First, time-resolved OKG signals were measured in CS₂. In Figure 6-3, the red open circles refer to the OKG signals using elliptically polarized probe light; the black solid squares as a reference refer to the general OKG signals using linearly polarized probe light. Both of the OKG signal intensity was normalized. The red circles agree well with the black squares. It indicates that the optical Kerr measurements we proposed based on light-induced polarization ellipse rotation using elliptically polarized probe light can do the ultrafast measurements as a general OKG.

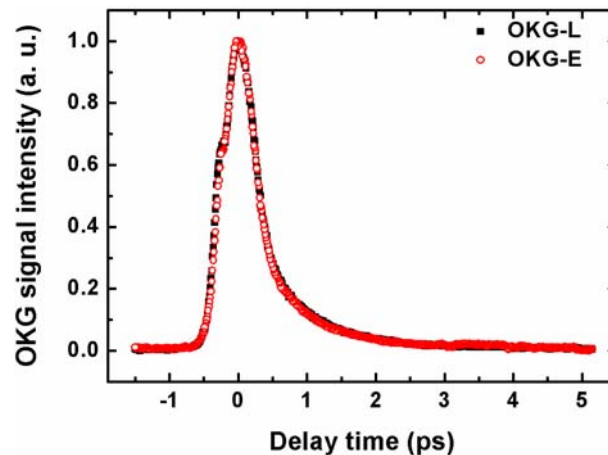


Figure 6-3: Time-resolved measurements of OKG signals in CS₂. The red open circles refer to the OKG signals using elliptically polarized probe light; the black solid squares as a reference refer to the general OKG signals using linearly polarized probe light.

In our experiments, we kept the pump fluence at about 4 mJ/cm² which would induce an average phase shift about $\pi/3$ in 1-mm CS₂. The probe beam was too weak to induce nonlinear effect. In Figure 6-4, scatter plots are experimental results; solid

lines are fitted curves using Eq. (6-5). Divided by the optimum OKG signal intensity, all the experimental data were normalized.

First, we studied the pump polarization direction dependence of OKG signal intensity under different polarization states of the probe beam (see Figure 6-4(a)). The angle α was fixed at 0° , 22.5° , and 45° , corresponding to linearly, elliptically, and circularly polarized probe beams, respectively. The different β values correspond to different pump polarizations directions. When $\alpha=0^\circ$, i. e. linearly polarized probe beam, the polarization dependence of the OKG signal intensity was just as that in a general OKG measurement [16], only when the polarization angle between the probe and pump is 45° , the OKG signal intensity can reach an optimum value. When $\alpha=22.5^\circ$, i. e. elliptically polarized probe beam, the pump polarization direction dependence of the OKG signal intensity curve was similar to that $\alpha=0^\circ$ but changed between 0.5 and 1. This result agrees with Eq. (6-5). In particular, when $\alpha=45^\circ$, i. e. circularly polarized probe beam, the OKG signal intensity stabilizes around the optimum value at any pump polarization angle. It verifies there will be no pump polarization direction restriction on the OKG signal intensity when the probe beam is circularly polarized.

In addition, to validate Eq. (6-5), the probe polarization state dependence of OKG signal intensity under different pump polarization directions (see Figure 6-4(b)) was investigated. The angle β was fixed at 0° , 22.5° , and 45° , corresponding to three different pump polarizations directions. In Figure 6-4 (b), the experimental results are consistent with the theoretical curves, which confirm Eq. (6-5).

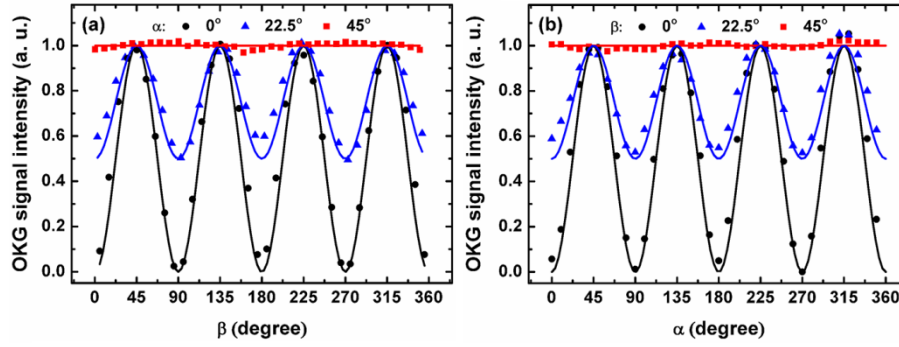


Figure 6-4: (a) Pump polarization direction dependence of OKG signal intensity under different polarization states of the probe beam. (b) Probe beam polarization state dependence of OKG signal intensity under different pump polarization directions. Scatter plots are experimental results; solid lines are fitted curves using Eq. (6-5).

6.5 Summary

In this chapter, we developed an OKG based on pump light induced probe polarization ellipse rotation. By introducing a pair of crossed quarter-wave plates in a general OKG, different polarization state of the probe beam, such as linearly, elliptically, and circularly polarized lights, can be obtained before focused into the Kerr medium. The theoretical formula of the OKG signal intensity was obtained by Jones calculus, and it was validated by the experimental results. It was found that the OKG signal intensity would reach an optimum value independent of the pump polarization direction when the probe beam was a circularly polarized light.

Chapter 7

Conclusions

The main focus of this thesis is on the development of single-shot optical Kerr effect measurements for imaging of the ultrafast laser pulses propagation in the transparent media, and the investigation of femtosecond time-resolved OKG measurements. The major contributions of this research are summarized below. And future work is also listed in this chapter.

7.1 Contributions

The major contributions of this thesis are outlined as follows:

- The ultrafast time-resolved single-shot imaging of femtosecond pulse propagation using a supercontinuum and FTOP in transparent liquids has been investigated [138,139]. The supercontinuum probe senses the instantaneous birefringence induced by the laser pulse, and a FTOP image with different color distributions could be obtained. By comparing the wavelength distributions and the saturation variation of the images, the recorded FTOP images in two samples with different response time were analyzed. In the fast response sample, N-methyl-2-pyrrolidone (NMP), the spectral widths and the saturation values of the FTOP image at fixed positions were narrower and higher than those in CS₂.

Due to the slow response of CS₂, the probe light sensed a long-lived birefringence and the FTOP image contained more wavelength components at every position along the pump pulse propagation direction.

- High-frame-rate observations of a single femtosecond laser pulse propagating intransparent medium using the FTOP and an echelon has been demonstrated [124,140]. The echelon produced a spatially encoded time delay for the probe pulse to capture directly four successive images of an intense propagating pulse with picosecond time interval and femtosecond time resolution. Using this method, we observed the propagation process of a single femtosecond laser pulse in fused silica with 280 fs time resolution and 1.05 THz frame rate. The influence of pulse-energy fluctuation on the spatial and temporal distribution of the single laser pulse was visualized using the single-shot measurements.
- The pump power dependence of the spatial gating properties of femtosecond OKG has been investigated using coaxial two-color optical Kerr measurements in CS₂ [141]. As the pump power increased, the spatial pattern of the optical Kerr signals changed from a Gaussian spot to a ring form, and then a spot surrounded by a concentric ring, successively. By comparing the experimental data with the calculation results and measuring the pump power dependence of the OKG signal intensity, we demonstrated that the spatial variation of OKG transmittance could be attributed to the non-uniform spatially distributed phase change of the probe beam, due to the transient birefringence effect induced by pump beam with transverse mode of a Gaussian distribution.
- Based on light-induced polarization ellipse rotation effect, an ultrafast OKG in which an elliptically polarized probe beam was used by introducing a pair of crossed quarter-wave plates before and after the Kerr medium in a conventional

OKG arrangement has been proposed. When the probe beam passed through the Kerr medium, a rotation of the polarization ellipse of the probe beam would occur due to the transient birefringence induced by the pump beam, and parts of the probe beam would pass through the OKG. Theoretical calculations and experimental results indicated that the OKG signal intensity would reach an optimum value and be pump-polarization independent when the probe beam were circularly polarized.

7.2 Future Work

There are two research topics in this area that can be possibly explored in the future:

- Combination of the techniques of supercontinuum probing with an echelon in single-shot pump-probe imaging: In the pump-probe spectroscopy, using a supercontinuum as the probe beam, and at the same time, introducing an echelon into the probe light path, thus a probe pulse can be subdivided into multiple distinct supercontinuum pulses with different time delay. Therefore, this technique can realize time- and wavelength-resolved pump-probe spectroscopy with high time resolution and large dynamic range which can be applied to measure the photochemical irreversible ultrafast dynamics.
- Investigation of the application of femtosecond time-resolved OKG measurements based on light-induced polarization ellipse rotation.

Bibliography

- [1] Duguay M, Hansen J-W. An ultrafast light gate[J]. Appl. Phys. Lett., 1969, 15(6): 192-194.
- [2] Righini R. Ultrafast optical kerr effect in liquids and solids[J]. Science, 1993, 262(5138): 1386-1390.
- [3] Yu Z, Gundlach L, Piotrowiak P. Efficiency and temporal response of crystalline Kerr media in collinear optical Kerr gating[J]. Optics Letters, 2011, 36(15): 2904-6.
- [4] Lee J Y, Yin L, Agrawal G P, et al. Ultrafast optical switching based on nonlinear polarization rotation in silicon waveguides[J]. Optics Express, 2010, 18(11): 11514-23.
- [5] Imakita K, Ito M, Naruiwa R, Fujii M, et al. Ultrafast third order nonlinear optical response of donor and acceptor codoped and compensated silicon quantum dots[J]. Applied Physics Letters, 2012, 101(4): 041112.
- [6] Kanematsu Y, Ozawa H, Tanaka I, et al. Femtosecond optical Kerr-gate measurement of fluorescence spectra of dye solutions[J]. J. Lumin., 2000, 87: 917-919.
- [7] Kinoshita S, Ozawa H, Kanematsu Y, et al. Efficient optical Kerr shutter for femtosecond time-resolved luminescence spectroscopy[J]. Rev. Sci. Instrum., 2000, 71(9): 3317-3322.
- [8] Wang F, Dukovic G, Brus LE, et al. Time-resolved fluorescence of carbon nanotubes and its implication for radiative lifetimes[J]. Phys. Rev. Lett., 2004, 92(17): 177401.
- [9] Takeda J, Nakajima K, Kurita S, et al. Time-resolved luminescence spectroscopy by the optical Kerr-gate method applicable to ultrafast relaxation processes [J].

- Physical Review B, 2000, 62(15): 10083.
- [10] Arzhantsev S, Maroncelli M. Design and characterization of a femtosecond fluorescence spectrometer based on optical Kerr gating [J]. Applied spectroscopy, 2005, 59(2): 206-220.
- [11] Liu H, Tan W, Si J, et al. Acquisition of gated spectra from a supercontinuum using ultrafast optical Kerr gate of lead phthalocyanine-doped hybrid glass [J]. Optics Express, 2008, 16(17) : 13486-13491.
- [12] Zhang H, Liu H, Si J, et al. Low threshold power density for the generation of frequency up-converted pulses in bismuth glass by two crossing chirped femtosecond pulses[J]. Optics express, 2011, 19(13): 12039-12044.
- [13] Appavoo K, Sfeir M Y. Enhanced broadband ultrafast detection of ultraviolet emission using optical Kerr gating [J]. Review of Scientific Instruments, 2014, 85(5): 055114.
- [14] Yoo K M, Xing Q, Alfano R R. Imaging objects hidden in highly scattering media using femtosecond second-harmonic-generation cross-correlation time gating [J]. Optics letters, 1991, 16(13): 1019-1021.
- [15] Tan W, Liu H, Si J, et al. Control of the gated spectra with narrow bandwidth from a supercontinuum using ultrafast optical Kerr gate of bismuth glass[J]. Applied Physics Letters, 2008, 93(5): 051109.
- [16] Fork R, Greene B, Shank C. Generation of optical pulses shorter than 0.1 psec by colliding pulse mode locking[J]. Appl. Phys. Lett., 1981, 38(9): 671-672.
- [17] Fork R, Shank C, Yen R. Amplification of 70-fs optical pulses to gigawatt powers[J]. Appl. Phys. Lett., 1982, 41(3): 223-225.
- [18] Spence DE, Kean PN, Sibbett W. 60-fsec pulse generation from a self-mode-locked Ti: sapphire laser[J]. Opt. lett., 1991, 16(1): 42-44.

- [19]Carbone F, Aubbock G, Cannizzo A, et al. Femtosecond carrier dynamics in bulk graphite and graphene paper[J]. Chem. Phys. Lett., 2011, 504(1-3): 37-40.
- [20]Barty A, Caleman C, Aquila A, et al. Self-terminating diffraction gates femtosecond X-ray nanocrystallography measurements[J]. Nat. Photonics, 2012, 6(1): 35-40.
- [21]Gabriel MM, Kirschbrown JR, Christesen JD, et al. Direct imaging of free carrier and trap carrier motion in silicon nanowires by spatially-separated femtosecond pump-probe microscopy[J]. Nano Lett., 2013, 13(3): 1336-1340.
- [22]Potemkin F, Mareev E. Dynamics of multiple bubbles, excited by a femtosecond filament in water[J]. Laser Phys. Lett., 2015, 12(1): 015405.
- [23]Schaffer C, Nishimura N, Glezer E, et al. Dynamics of femtosecond laser-induced breakdown in water from femtoseconds to microseconds[J]. Opt. Express, 2002, 10(3): 196-203.
- [24]Huang D, Swanson EA, Lin CP, et al. Optical coherence tomography[J]. Science, 1991, 254(5035): 1178-1181.
- [25]Xu L, Zhang XC, Auston D. Terahertz beam generation by femtosecond optical pulses in electro - optic materials[J]. Appl. Phys. Lett., 1992, 61(15): 1784-1786.
- [26]Hirori H, Doi A, Blanchard F, et al. Single-cycle terahertz pulses with amplitudes exceeding 1 MV/cm generated by optical rectification in LiNbO₃[J]. Appl. Phys. Lett., 2011, 98(9): 091106.
- [27]Liu M, Hwang HY, Tao H, et al. Terahertz-field-induced insulator-to-metal transition in vanadium dioxide metamaterial[J]. Nature, 2012, 487(7407): 345-348.
- [28]Kawata S, Sun H-B, Tanaka T, et al. Finer features for functional microdevices[J]. Nature, 2001, 412(6848): 697-698.

- [29] Ushiba S, Shoji S, Masui K, et al. 3D microfabrication of single-wall carbon nanotube/polymer composites by two-photon polymerization lithography[J]. *Carbon*, 2013, 59: 283-288.
- [30] Dudley J M, Genty G, Coen S. Supercontinuum generation in photonic crystal fiber [J]. *Reviews of modern physics*, 2006, 78(4): 1135.
- [31] Couairon A, Mysyrowicz A. Femtosecond filamentation in transparent media [J]. *Physics reports*, 2007, 441(2): 47-189.
- [32] Bukin OA, Babii MY, Golik SS, et al. Lidar sensing of the atmosphere with gigawatt laser pulses of femtosecond duration[J]. *Quantum Electron.*, 2014, 44(6): 563-569.
- [33] Chagas JCS, Leisner T, Kasparian J. Pump-probe differential Lidar to quantify atmospheric supersaturation and particle-forming trace gases[J]. *Appl. Phys. B*, 2014, 117(2): 667-672.
- [34] Petrarca M, Henin S, Berti N, et al. White-light femtosecond Lidar at 100 TW power level[J]. *Appl. Phys. B*, 2014, 114(3): 319-325.
- [35] Bourayou R, Méjean G, Kasparian J, et al. White-light filaments for multiparameter analysis of cloud microphysics[J]. *J. Opt. Soc. Am. B: Opt. Phys.*, 2005, 22(2): 369-377.
- [36] Kasparian J, Rodriguez M, Méjean G, et al. White-light filaments for atmospheric analysis [J]. *Science*, 2003, 301(5629): 61-64.
- [37] Luo Q, Xu H, Hosseini S, et al. Remote sensing of pollutants using femtosecond laser pulse fluorescence spectroscopy[J]. *Appl. Phys. B*, 2006, 82(1): 105-109.
- [38] Ackermann R, Stelmaszczyk K, Rohwetter P, et al. Triggering and guiding of megavolt discharges by laser-induced filaments under rain conditions[J]. *Appl. Phys. Lett.*, 2004, 85(23): 5781-5783.

- [39] Ackermann R, Méchain G, Méjean G, et al. Influence of negative leader propagation on the triggering and guiding of high voltage discharges by laser filaments[J]. *Appl. Phys. B*, 2006, 82(4): 561-566.
- [40] Chin S, Wang T-J, Marceau C, et al. Advances in intense femtosecond laser filamentation in air[J]. *Laser Phys.*, 2012, 22(1): 1-53.
- [41] Mitryukovskiy S I, Liu Y, Prade B, et al. Coherent synthesis of terahertz radiation from femtosecond laser filaments in air[J]. *Applied Physics Letters*, 2013, 102(22): 221107.
- [42] Minardi S, Gopal A, Tatarakis M, et al. Time-resolved refractive index and absorption mapping of light-plasma filaments in water [J]. *Optics Letters*, 2008, 33(1):86-8.
- [43] Balciunas T, Melninkaitis A, Tamosauskas G, et al. Time-resolved off-axis digital holography for characterization of ultrafast phenomena in water [J]. *Optics Letters*, 2008, 33(1):58-60.
- [44] Centurion M, Pu Y, Psaltis D. Holographic capture of femtosecond pulse propagation [J]. *Journal of Applied Physics*, 2006, 100(6): 063104-9 .
- [45] Kubota T, Komai K, Yamagiwa M, et al. Moving picture recording and observation of three-dimensional image of femtosecond light pulse propagation [J]. *Optics Express*, 2007, 15(22): 14348-54.
- [46] Mermillod-Blondin A, Mauclair C, Bonse J, et al. Time-resolved imaging of laser-induced refractive index changes in transparent media [J]. *Review of Scientific Instruments*, 2011, 82(3): 033703-8.
- [47] Fujimoto M, Aoshima S, Hosoda M, et al. Femtosecond time-resolved optical polarigraphy: imaging of the propagation dynamics of intense light in a medium [J]. *Optics letters*, 1999, 24(12): 850-852.

- [48] Kumagai H, Cho S H, Ishikawa K, et al. Observation of the complex propagation of a femtosecond laser pulse in a dispersive transparent bulk material [J]. *JOSA B*, 2003, 20(3): 597-602.
- [49] Hosoda M, Aoshima S, Fujimoto M, et al. Femtosecond snapshot imaging of propagating light itself [J]. *Applied optics*, 2002, 41(12): 2308-2317.
- [50] Ma L, Zhang K, Kloc C, et al. Singlet fission in rubrene single crystal: direct observation by femtosecond pump-probe spectroscopy [J]. *Phys. Chem. Chem. Phys.*, 2012, 14(23): 8307-8312.
- [51] Tzallas P, Skantzakis E, Nikolopoulos L, et al. Extreme-ultraviolet pump-probe studies of one-femtosecond-scale electron dynamics [J]. *Nature Phys.*, 2011, 7(10): 781-784.
- [52] Woutersen S, Emmerichs U, Bakker H. Femtosecond mid-IR pump-probe spectroscopy of liquid water: Evidence for a two-component structure [J]. *Science*, 1997, 278(5338): 658-660.
- [53] Dong C, Buehler C, So PT, et al. Implementation of intensity-modulated laser diodes in time-resolved, pump-probe fluorescence microscopy [J]. *Appl. Opt.*, 2001, 40(7): 1109-1115.
- [54] Scherer N, Ruggiero A, Du M, et al. Time resolved dynamics of isolated molecular systems studied with phase - locked femtosecond pulse pairs [J]. *J. Chem. Phys.*, 1990, 93(1): 856-857.
- [55] Kikuchi K, Kakui M, Zah C-E, et al. Observation of highly nondegenerate four-wave mixing in 1.5 μm traveling-wave semiconductor optical amplifiers and estimation of nonlinear gain coefficient [J]. *IEEE J. Quantum Electron.*, 1992, 28(1): 151-156.
- [56] Materny A, Chen T, Schmitt M, et al. Wave packet dynamics in different

- electronic states investigated by femtosecond time-resolved four-wave-mixing spectroscopy[J]. *Appl. Phys. B*, 2000, 71(3): 299-317.
- [57]d'Abzac F-X, Kervella M, Hespel L, et al. Experimental and numerical analysis of ballistic and scattered light using femtosecond optical Kerr gating: a way for the characterization of strongly scattering media[J]. *Opt. Express*, 2012, 20(9): 9604-9615.
- [58]McMorrow D, Lotshaw WT, Kenney-Wallace GA. Femtosecond optical Kerr studies on the origin of the nonlinear responses in simple liquids[J]. *IEEE J. Quantum Electron.*, 1988, 24(2): 443-454.
- [59]Kane DJ, Trebino R. Single-shot measurement of the intensity and phase of an arbitrary ultrashort pulse by using frequency-resolved optical gating[J]. *Opt. lett.*, 1993, 18(10): 823-825.
- [60]DeLong K, Trebino R, Hunter J, et al. Frequency-resolved optical gating with the use of second-harmonic generation[J]. *J. Opt. Soc. Am. B: Opt. Phys.*, 1994, 11(11): 2206-2215.
- [61]DeLong K, Trebino R, Kane DJ. Comparison of ultrashort-pulse frequency-resolved-optical-gating traces for three common beam geometries[J]. *J. Opt. Soc. Am. B: Opt. Phys.*, 1994, 11(9): 1595-1608.
- [62]Fittinghoff DN, Walmsley IA, Bowie JL, et al. Measurement of the intensity and phase of ultraweak, ultrashort laser pulses[J]. *Opt. lett.*, 1996, 21(12): 884-886.
- [63]Trebino R, DeLong KW, Fittinghoff DN, et al. Measuring ultrashort laser pulses in the time-frequency domain using frequency-resolved optical gating[J]. *Rev. Sci. Instrum.*, 1997, 68(9): 3277-3295.
- [64]Gu X, Xu L, Kimmel M, et al. Frequency-resolved optical gating and single-shot spectral measurements reveal fine structure in microstructure-fiber continuum[J].

- Opt. Lett., 2002, 27(13): 1174-1176.
- [65] Shirai H, Nomura Y, Fuji T. Real-time waveform characterization by using frequency-resolved optical gating capable of carrier-envelope phase determination[J]. IEEE Photonics J., 2014, 6(3):300212.
- [66] Shan J, Weling AS, Knoesel E, et al. Single-shot measurement of terahertz electromagnetic pulses by use of electro-optic sampling[J]. Opt. Lett., 2000, 25(6): 426-428.
- [67] Takeuchi S, Tahara T. Time-wavelength two-dimensional femtosecond fluorescence imaging[J]. Opt. Lett., 2004, 29(3): 313-315.
- [68] Furukawa N, Mair CE, Kleiman VD, et al. Femtosecond real-time pump-probe imaging spectroscopy[J]. Appl. Phys. Lett., 2004, 85(20): 4645-4647.
- [69] Makishima Y, Furukawa N, Ishida A, et al. Femtosecond real-time pump-probe imaging spectroscopy implemented on a single shot basis[J]. Jpn. J. Appl. Phys., 2006, 45(7R): 5986.
- [70] Chapman HN, Barty A, Bogan MJ, et al. Femtosecond diffractive imaging with a soft-X-ray free-electron laser[J]. Nat. Phys., 2006, 2(12): 839-843.
- [71] Ravasio A, Gauthier D, Maia F, et al. Single-shot diffractive imaging with a table-top femtosecond soft x-ray laser-harmonics source[J]. Phys. Rev. Lett., 2009, 103(2): 028104.
- [72] Wang T, Zhu D, Wu B, et al. Femtosecond single-shot imaging of nanoscale ferromagnetic order in Co/Pd multilayers using resonant x-ray holography[J]. Phys. Rev. Lett., 2012, 108(26): 267403.
- [73] Wesch S, Schmidt B, Behrens C, et al. A multi-channel THz and infrared spectrometer for femtosecond electron bunch diagnostics by single-shot spectroscopy of coherent radiation[J]. Nucl. Instrum. Methods Phys. Res., Sect.

- A, 2011, 665: 40-47.
- [74]Matlis N, Axley A, Leemans W. Single-shot ultrafast tomographic imaging by spectral multiplexing[J]. Nat. commun., 2012, 3: 1111.
- [75]Li Z, Zgadzaj R, Wang X, et al. Single-shot tomographic movies of evolving light-velocity objects[J]. Nat. commun., 2014, 5.
- [76]Jiang Z, Zhang X-C. Electro-optic measurement of THz field pulses with a chirped optical beam[J]. Appl. Phys. Lett., 1998, 72(16): 1945-1947.
- [77]Berden G, Jamison SP, MacLeod AM, et al. Electro-optic technique with improved time resolution for real-time, nondestructive, single-shot measurements of femtosecond electron bunch profiles[J]. Phys. Rev. Lett., 2004, 93(11): 114802.
- [78]Okayasu Y, Tomizawa H, Matsubara S, et al. Feasibility study of a single-shot 3D electron bunch shape monitor with an electro-optic sampling technique[J]. Phys. Rev. Spec. TOP-AC., 2013, 16(5): 052801.
- [79]Alfano R, Shapiro S. Observation of self-phase modulation and small-scale filaments in crystals and glasses[J]. Phys. Rev. Lett., 1970, 24(11): 592.
- [80]Alfano R, Shapiro S. Emission in the region 4000 to 7000 Å via four-photon coupling in glass[J]. Phys. Rev. Lett., 1970, 24(11): 584.
- [81]Chin SL, Petit S, Borne F, et al. The white light supercontinuum is indeed an ultrafast white light laser[J]. Jpn. J Appl. Phys., 1999, 38(2A): L126.
- [82]Kasparian J, Sauerbrey R, Mondelain D, et al. Infrared extension of the supercontinuum generated by femtosecond terawatt laser pulses propagating in the atmosphere[J]. Opt. Lett., 2000, 25(18): 1397-1399.
- [83]Corkum P, Rolland C, Srinivasan-Rao T. Supercontinuum generation in gases[J]. Phys. Rev. Lett., 1986, 57(18): 2268.

- [84]Kuyken B, Liu X, Osgood Jr RM, et al. Mid-infrared to telecom-band supercontinuum generation in highly nonlinear silicon-on-insulator wire waveguides[J]. *Opt. Express*, 2011, 19(21): 20172-20181.
- [85]Liu X, Lu X, Liu X, et al. Broadband supercontinuum generation in air using tightly focused femtosecond laser pulses[J]. *Opt. Lett.*, 2011, 36(19): 3900-3902.
- [86]Marandi A, Rudy CW, Plotnichenko VG, et al. Mid-infrared supercontinuum generation in tapered chalcogenide fiber for producing octave-spanning frequency comb around 3 μm [J]. *Opt. Express*, 2012, 20(22): 24218-24225.
- [87]Silva F, Austin D, Thai A, et al. Multi-octave supercontinuum generation from mid-infrared filamentation in a bulk crystal[J]. *Nat. Commun.*, 2012, 3: 807.
- [88]Jukna V, Galinis J, Tamosauskas G, et al. Infrared extension of femtosecond supercontinuum generated by filamentation in solid-state media[J]. *Appl. Phys. B*, 2014, 116(2): 477-483.
- [89]Vasa P, Dharmadhikari JA, Dharmadhikari AK, et al. Supercontinuum generation in water by intense, femtosecond laser pulses under anomalous chromatic dispersion[J]. *Phys. Rev. A*, 2014, 89(4): 043834.
- [90]Xu H, Daigle J, Luo Q, et al. Femtosecond laser-induced nonlinear spectroscopy for remote sensing of methane[J]. *Appl. Phys. B*, 2006, 82(4): 655-658.
- [91] Daigle J-F, Kamali Y, Châteauneuf M, et al. Remote sensing with intense filaments enhanced by adaptive optics[J]. *Appl. Phys. B*, 2009, 97(3): 701-713.
- [92] Wang T-J, Xu H, Daigle J-F, et al. Water vapor concentration measurement in air using filament-induced fluorescence spectroscopy[J]. *Opt. Lett.*, 2012, 37(10): 1706-1708.
- [93] Povazay B, Bizheva K, Unterhuber A, et al. Submicrometer axial resolution optical coherence tomography[J]. *Opt. Lett.*, 2002, 27(20): 1800-1802.

- [94] Tomlins PH, Wang R. Theory, developments and applications of optical coherence tomography[J]. *J. Phys. D: Appl. Phys.*, 2005, 38(15): 2519.
- [95] Schenkel B, Biegert J, Keller U, et al. Generation of 3.8-fs pulses from adaptive compression of a cascaded hollow fiber supercontinuum[J]. *Opt. Lett.*, 2003, 28(20): 1987-1989.
- [96] Zhang W, Teng H, Yun C, et al. Generation of sub-2 cycle optical pulses with a differentially pumped hollow fiber[J]. *Chinese Phys. Lett.*, 2010, 27(5): 054211.
- [97] Tan W, Yang Y, Si J, et al. Shape measurement of objects using an ultrafast optical Kerr gate of bismuth glass[J]. *J. Appl. Phys.*, 2010, 107(4): 043104-043104-043103.
- [98] Zhang L, Xin X, Liu B, et al. OFDM modulated WDM-ROF system based on PCF-Supercontinuum[J]. *Opt. Express*, 2010, 18(14): 15003-15008.
- [99] Kovalenko S, Ruthmann J, Ernsting N. Femtosecond hole-burning spectroscopy with stimulated emission pumping and supercontinuum probing[J]. *J. Chem. Phys.*, 1998, 109(5): 1894-1900.
- [100] Kovalenko S, Dobryakov A, Ruthmann J, et al. Femtosecond spectroscopy of condensed phases with chirped supercontinuum probing[J]. *Phys. Rev. A*, 1999, 59(3): 2369.
- [101] Naumov A, Zheltikov A. Frequency–time and time–space mappings with broadband and supercontinuum chirped pulses in coherent wave mixing and pump–probe techniques[J]. *Appl. Phys. B*, 2003, 77(2-3): 369-376.
- [102] Dobryakov A, Kovalenko S, Weigel A, et al. Femtosecond pump/supercontinuum-probe spectroscopy: optimized setup and signal analysis for single-shot spectral referencing[J]. *Rev. Sci. Instrum.*, 2010, 81(11): 113106.
- [103] Krebs N, Pugliesi I, Hauer J, et al. Two-dimensional Fourier transform

- spectroscopy in the ultraviolet with sub-20 fs pump pulses and 250–720 nm supercontinuum probe[J]. *New J. Phys.*, 2013, 15(8): 085016.
- [104] Kanal F, Keiber S, Eck R, et al. 100-kHz shot-to-shot broadband data acquisition for high-repetition-rate pump–probe spectroscopy[J]. *Opt. Express*, 2014, 22(14): 16965-16975.
- [105] Dietzek B, Kiefer W, Hermann G, et al. Solvent effects on the excited-state processes of protochlorophyllide: a femtosecond time-resolved absorption study[J]. *J. Phys. Chem. B*, 2006, 110(9): 4399-4406.
- [106] Schmitt M, Dietzek B, Hermann G, et al. Femtosecond time-resolved spectroscopy on biological photoreceptor chromophores[J]. *Laser Photon. Rev.*, 2007, 1(1): 57-78.
- [107] Dooley CJ, Dimitrov SD, Fiebig T. Ultrafast Electron Transfer Dynamics in CdSe/CdTe Donor– Acceptor Nanorods[J]. *J. Phys. Chem. C*, 2008, 112(32): 12074-12076.
- [108] Dimitrov SD, Dooley CJ, Trifonov AA, et al. Femtosecond probing of optical phonon dynamics in quantum-confined CdTe nanocrystals[J]. *J. Phys. Chem. C*, 2009, 113(10): 4198-4201.
- [109] Styers-Barnett DJ, Ellison SP, Mehl BP, et al. Exciton dynamics and biexciton formation in single-walled carbon nanotubes studied with femtosecond transient absorption spectroscopy[J]. *J. Phys. Chem. C*, 2008, 112(12): 4507-4516.
- [110] Tan W, Tong J, Si J, et al. High time-resolved three-dimensional imaging using ultrafast optical Kerr gate of bismuth glass[J]. *IEEE Photonics Technol. Lett.*, , 2011, 23(8): 471-473.
- [111] Wakeham GP, Chung DD, Nelson KA. Femtosecond time-resolved spectroscopy of energetic materials[J]. *Thermochim. Acta*, 2002, 384(1): 7-21.

- [112] Wakeham GP, Nelson KA. Dual-echelon single-shot femtosecond spectroscopy[J]. *Opt. Lett.*, 2000, 25(7): 505-507.
- [113] Poulin PR, Nelson KA. Irreversible organic crystalline chemistry monitored in real time[J]. *Science*, 2006, 313(5794): 1756-1760.
- [114] Minami Y, Hayashi Y, Takeda J, et al. Single-shot measurement of a terahertz electric-field waveform using a reflective echelon mirror[J]. *Appl. Phys. Lett.*, 2013, 103(5): 051103.
- [115] Kim K, Yellampalle B, Taylor A, et al. Single-shot terahertz pulse characterization via two-dimensional electro-optic imaging with dual echelons[J]. *Opt. Lett.*, 2007, 32(14): 1968-1970.
- [116] Shin T, Wolfson JW, Teitelbaum SW, et al. Dual echelon femtosecond single-shot spectroscopy[J]. *Rev. Sci. Instrum.*, 2014, 85(8): 083115.
- [117] Sakaibara H, Ikegaya Y, Katayama I, et al. Single-shot time-frequency imaging spectroscopy using an echelon mirror[J]. *Opt. Lett.*, 2012, 37(6): 1118-1120.
- [118] Kanbara H, Kobayashi H, Kaino T, et al. Highly efficient ultrafast optical Kerr shutters with the use of organic nonlinear materials [J]. *Josa B*, 1994, 11(11):2216-2223.
- [119] Dota K, Dharmadhikari J A, Mathur D, et al. Third-order nonlinear optical response in transparent solids using ultrashort laser pulses[J]. *Applied Physics B Lasers & Optics*, 2012, 107(3): 703-709.
- [120] Schmidt B, Laimgruber S, Zinth W, et al. A broadband Kerr shutter for femtosecond fluorescence spectroscopy[J]. *Applied Physics B Lasers & Optics*, 2003, 76(8): 809-814.
- [121] Yan L H, Yue J J, Si J H, et al. Influence of self-diffraction effect on

- femtosecond pump-probe optical Kerr measurements[J]. *Optics Express*, 2008, 16(16):12069-74.
- [122] Takeda J, Nakajima K, Kurita S, et al. Time-resolved luminescence spectroscopy by the optical Kerr-gate method applicable to ultrafast relaxation processes[J]. *Phys. Rev. B*, 2000, 62(15): 10083.
- [123] Fujimoto M, Aoshima S, Tsuchiya Y. Multiframe observation of an intense femtosecond optical pulse propagating in air [J]. *Optics letters*, 2002, 27(5): 309-311.
- [124] Yan L, Yue J, Si J, et al. Polarization Dependence of Femtosecond Optical Kerr Signals in Bismuth Glasses[J]. *IEEE Photonics Technol. Lett.*, , 2009, 21(21): 1606-1608.
- [125] Kalpouzos C, Lotshaw W T, McMorro D, et al. Femtosecond laser-induced Kerr responses in liquid carbon disulfide [J]. *Journal of Physical Chemistry*, 1987, 91(8): 2028-2030.
- [126] Greene B I, Farrow R C. The subpicosecond kerr effect in CS₂ [J]. *Chemical Physics Letters*, 1983, 98(3): 273-276.
- [127] Li J, Wang S, Yang H, et al. Femtosecond third-order optical nonlinearity of C₆₀ and its derivative at a wavelength of 810 nm [J]. *Chemical physics letters*, 1998, 288(2): 175-178.
- [128] Brodeur A, Chin S L. Ultrafast white-light continuum generation and self-focusing in transparent condensed media [J]. *JOSA B*, 1999, 16(4): 637-650.
- [129] Hu X, Wang Y, Zhao W, et al. Nonlinear chirped-pulse propagation and supercontinuum generation in photonic crystal fibers [J]. *Applied optics*, 2010, 49(26): 4984-4989.

- [130] Nagura C, Suda A, Kawano H, et al. Generation and characterization of ultrafast white-light continuum in condensed media [J]. *Applied optics*, 2002, 41(18): 3735-3742.
- [131] Matlis N H, Axley A, Leemans W P. Single-shot ultrafast tomographic imaging by spectral multiplexing [J]. *Nature Communications*, 2012, 3(1): 301-303.
- [132] Li Z, Zgadzaj Z, Wang X, Chang Y, et al. Single-shot tomographic movies of evolving light-velocity objects.[J]. *Nature Communications*, 2014, 5(2): 1661-1667.
- [133] Barty A, Boutet S, Bogan M J, et al. Ultrafast single-shot diffraction imaging of nanoscale dynamics [J]. *Nature Photonics*, 2008, 2(7): 415-419.
- [134] Wang T, Zhu D, Wu B, et al. Femtosecond single-shot imaging of nanoscale ferromagnetic order in Co/Pd multilayers using resonant x-ray holography [J]. *Physical Review Letters*, 2012, 108(26):1-5.
- [135] Fujimoto M, Aoshima S I, Hosoda M, et al. Analysis of instantaneous profiles of intense femtosecond optical pulses propagating in helium gas measured by using femtosecond time-resolved optical polarigraphy [J]. *Physical Review A*, 2001, 64(3): 033813.
- [136] Yan L, Wang X, Si J, et al. Multi-Frame Observation of a Single Femtosecond Laser Pulse Propagation Using an Echelon and Optical Polarigraphy Technique [J]. *IEEE Photonics Technology Letters*, 2013, 25(19): 1879-1881.
- [137] Oudar J. L., Coherent phenomena involved in the time-resolved optical Kerr effect [J]. *IEEE Journal of Quantum Electronics*, 1983, 19(4): 713-718.
- [138] Wang X F, Si J H, Yan L H, et al. Ultrafast single-shot imaging of femtosecond pulse propagation in transparent liquids using a supercontinuum and optical polarigraphy[J]. *J. Opt.*, 2014, 16(1): 015203.

- [139] Yan L H, Wang X F, Si J H, et al. Time-resolved single-shot imaging of femtosecond laser induced filaments using supercontinuum and optical polarigraphy[J]. *Appl. Phys. Lett.*, 2012, 100(11): 111107-3.
- [140] Wang X F, Yan L H, Si J H, et al. High-frame-rate observation of single femtosecond laser pulse propagation in fused silica using an echelon and optical polarigraphy technique[J]. *Appl. Opt.*, 2014, 53(36): 8395-8399.
- [141] Wang X F, He P C, Yan L H, et al. Pump power dependence of the spatial gating properties of femtosecond optical Kerr effect measurements[J]. *Appl. Phys. B*, 2013, 112(2): 279-283.